Geophysical Journal International

Geophys. J. Int. (2021) **224,** 1079–1095
Advance Access publication 2020 October 23
GJI Geomagnetism, Rock Magnetism and Palaeomagnetism

doi: 10.1093/gji/ggaa506

Records of the Laschamps geomagnetic polarity excursion from Black Sea sediments: magnetite versus greigite, discrete sample versus U-channel data

Norbert R. Nowaczyk [1], Jiabo Liu*[,1] and Helge W. Arz[2]

[1] *Helmholtz Centre Potsdam, GFZ German Research Centre for Geosciences, Section Paleoclimate and Landscape evolution,* 14473 *Potsdam, Germany. E-mail: nowa@gfz-potsdam.de*
[2] *Leibniz Institute for Baltic Sea Research Warnemünde,* 18119 *Rostock, Germany*

Accepted 2020 October 15. Received 2020 October 15; in original form 2020 May 26

SUMMARY

Magnetostratigraphic investigation of sediment cores from two different water depths in the SE Black Sea based on discrete samples, and parallel U-channels in one of the cores, yielded high-resolution records of geomagnetic field variations from the past about 68 ka. Age constrains are provided by three tephra layers of known age, accelerator mass spectrometry ^{14}C dating, and by tuning element ratios obtained from X-ray fluorescence scanning to the oxygen isotope record from Greenland ice cores. Sedimentation rates vary from a minimum of ∼5 cm ka^{-1} in the Holocene to a maximum of ∼50 cm ka^{-1} in glacial marine isotope stage 4. Completely reversed inclinations and declinations as well as pronounced lows in relative palaeointensity around 41 ka provide evidence for the Laschamps geomagnetic polarity excursion. In one of the investigated cores also a fragmentary record of the Mono Lake excursion at 34.5 ka could be revealed. However, the palaeomagnetic records are more or less affected by greigite, a diagenetically formed magnetic iron sulphide. By definition of an exclusion criterion based on the ratio of saturation magnetization over volume susceptibility, greigite-bearing samples were removed from the palaeomagnetic data. Thus, only 25–55 per cent of the samples were left in the palaeomagnetic records obtained from sediments from the shallower coring site. The palaeomagnetic record from the deeper site, based on both discrete samples and U-channels, is much less affected by greigite. The comparison of palaeomagnetic data shows that the major features of the Laschamps polarity excursion were similarly recovered by both sampling techniques. However, several intervals had to be removed from the U-channel record due to the presence of greigite, carrying anomalous directions. By comparison to discrete sample data, also some directional artefacts in the U-channel record, caused by low-pass filtering of the broad magnetometer response functions, averaging across fast directional and large amplitude changes, can be observed. Therefore, high-resolution sampling with discrete samples should be the preferred technique when fast geomagnetic field variations, such as reversals and excursions, shall be studied from sedimentary records in the very detail.

Key words: Magnetic properties; Geomagnetic excursions; Magnetostratigraphy; Palaeointensity; Palaeomagnetism.

1 INTRODUCTION

Geomagnetic field variations are an expression of short- to long-term geodynamo processes inside the Earth's liquid outer core (e.g. Merrill & McFadden 1999; Roberts 2008). Volcanic rocks, lacustrine and marine sediments, as well as archaeological artefacts can serve as recorders of these field variations, comprising palaeosecular variation, excursions, reversals, chrons and superchrons. The first geomagnetic excursion reported to have occurred in the Brunhes Chron is the Laschamps excursion, named after its type-locality close to the village 'Laschamps' in the Massif Central, France (Bonhommet & Babkine 1967; Gillot *et al.* 1979; Guillou *et al.* 2004;

*Now at: Southern University of Science and Technology, Department of Ocean Science and Engineering, 518055 Shenzhen, China.

Plenier *et al.* 2007; Nowaczyk *et al.* 2012; Laj *et al.* 2014, Channell *et al.* 2020). Concerning the naming of this excursion we now follow Kornprobst & Lénat (2019), pointing out that 'Laschamps' is the correct spelling, though in most publications up to now and even some official maps the 's' at the end has been notoriously omitted, for whatever reason. Since the discovery of the Laschamps excursion, further excursions have been reported in literature. A recent summary on geomagnetic excursions throughout the whole Quaternary is provided by Channell *et al.* (2020).

In order to interpret geomagnetic field behaviour correctly, it is of essential importance to be sure that obtained records of palaeomagnetic directions and/or (relative) palaeointensity are free of biases. In the case of sediments early diagenesis is one of the major processes affecting the quality of palaeomagnetic information. Either by partly or completely erasing the primary magnetic fraction and/or by the precipitation of a post-depositional, that is, a secondary magnetic mineral phase, often of unknown age, the palaeomagnetic information can become useless to a larger or lesser degree. The impact of these geochemical processes is best recognized in environments where preservation and dissolution of the magnetic fraction alternate periodically, for example due to orbital cycles, such as in the Mediterranean Sea (e.g. Dekkers *et al.* 1994) or the El'gygytgyn impact crater lake (Nowaczyk *et al.* 2013b). In various anoxic environments, dissolution of magnetite (Fe_3O_4) and the subsequent precipitation of greigite (Fe_3S_4) is a common process (e.g. Snowball & Thompson 1988; Ron *et al.* 2007; Nowaczyk 2011; Roberts *et al.* 2011).

In this paper, we discuss palaeomagnetic records obtained from greigite-affected sediment cores that were recovered from two different water depths in the SE Black Sea. In the cores from both sites, records of the Laschamps excursion could be revealed by high-resolution sampling with discrete samples. One core from the deeper site, less affected by greigite, was also sampled with U-channels.

Since the invention of so-called 'pass-through' or 'long-core magnetometers', the application of U-channels in magnetostratigraphy of long sedimentary sequences became a common procedure, mainly in the international ocean and continental deep-drilling programs. Especially the construction of magnetometers with a high-resolution pick-up system (Nagy & Valet 1993; Weeks *et al.* 1993) was a big step forward in studying long sediment sequences also in terms of using the data not just for dating purposes but also for the investigation of short-term geomagnetic field variations. However, by the pass-through technique palaeomagnetic information always gets convolved with the sensors' response functions. Thus, any U-channel record reflects a smoothed, more or less low-pass filtered record, depending on the half-width of the sensors' response functions. In order to recover at least a part of the high-frequency spectrum several deconvolution techniques have been developed (Oda & Shibuya 1996; Guyodo *et al.* 2002; Jackson *et al.* 2010; Oda & Xuan 2014; Xuan & Oda 2015; Xuan & Oda 2019). Anyway, the U-channel technique has some limitations (Brachfeld *et al.* 2004; Roberts 2006). Based on a detailed comparison of remanence measurements of artificial discrete samples and U-channels Philippe *et al.* (2018) even raised the question whether palaeomagnetic records from U-channels are appropriate at all for studying short-term geomagnetic field behaviour, such as reversals and excursions. For this study, due to the availability of four parallel cores from site M72/5–22 (Fig. 1), it was decided to check how data from a high-resolution sampling of the Laschamps excursion with discrete samples (Nowaczyk *et al.* 2012) compare to results from a parallel U-channel record from core M72/5–22GC4. Though analysed with a magnetometer with pick-up coils designed for high homogeneity instead for high-resolution, that is, it has wide sensor response functions, the results were expected to be insightful to some degree. One specific question was, how does the presence of greigite in a U-channel affects the measured data.

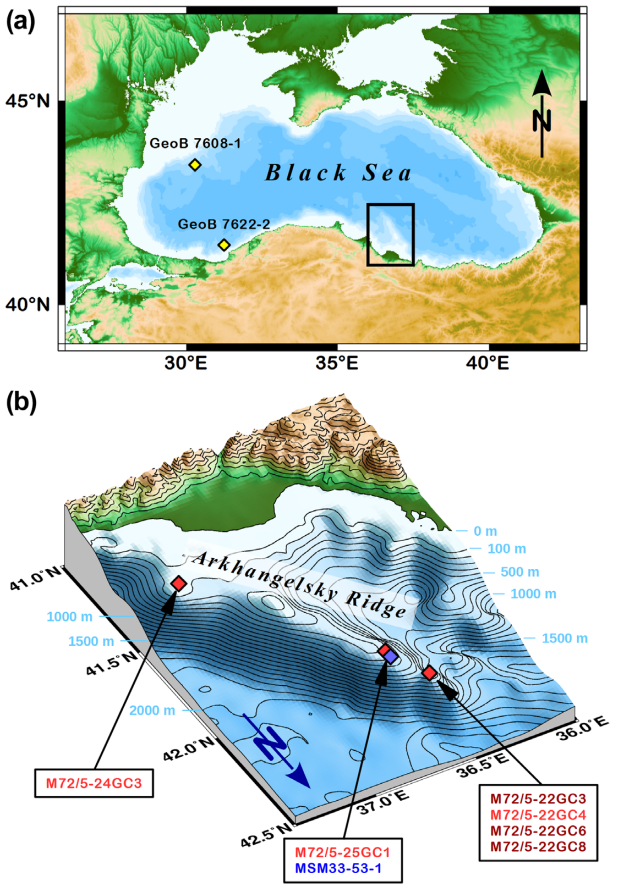

Figure 1. Core locations in (a) the SE Black Sea with (b) a more detailed perspective view of the Arkhangelsky Ridge (black rectangle in a). Yellow diamonds mark sites of cores recovered during *RV Meteor* expedition M51/4 in 2001, red diamonds and codes refer to cores recovered during *RV Meteor* expedition M72/5 in 2007, the blue diamond and code refers to a core recovered during *RV Maria S. Merian* expedition MSM33 in 2013. Bathymetric lines are shown every 100 m.

2 MATERIAL AND METHODS

2.1 Sediments under investigation

For this study, core MSM33–53-1 was subjected to a detailed palaeo- and rock magnetic investigation. It was recovered from a water depth of 443.4 m at the Arkhangelsky Ridge in the SE Black Sea during ship expedition MSM33 of German research vessel *RV Maria S. Merian* in 2013 (Fig. 1, Table 1). Sediments in the 797-cm-long core MSM33–53-1 cover the Holocene, marine isotope stage (MIS) 1, and most of the last glacial from MIS 2 to 4. For most of the time documented in core MSM33–53-1, until the early Holocene, the Black Sea was disconnected from the Mediterranean Sea. Its water level then was up to -100 m below modern sea level (e.g. Major *et al.* 2006; Shumilovskikh *et al.* 2012). At the study site fine-grained siliciclastic sediments with variable carbonate content (25–40 per cent, Nowaczyk *et al.* 2012) were deposited under limnic

Table 1. Location data of cores recovered from the Black Sea during *RV Meteor* expeditions M51/4 (2001), M72/5 (2007) and *RV Maria S. Merian* expedition MSM33 (2013), and list of related palaeomagnetic studies.

Core number	Site latitude	Site longitude	Water depth [m]	Core length [cm]	References
M72/5–24GC3	41° 28.66′ N	37° 11.68′ E	208.0	885	1,2,3,5,6
MSM33–55-1 PC	41° 54.01′ N	36° 46.98′ E	362.4	948	3,4,5,6,b
MSM33–56-1	41° 47.33′ N	36° 55.81‘ E	373.9	736	6,b
MSM33–57-1	41° 47.38′ N	36° 55.95‘ E	374.0	778	3,5,6,b
MSM33–54-3 PC	41° 58.99′ N	36° 43.85′ E	382.2	953	3,4,5,6,b
M72/5–25GC1	**42° 06.21′ N**	**36° 37.43′ E**	**418.0**	**952**	**1,2,3,5,6,a**
MSM33–51-3 PC	42° 02.38′ N	36° 43.08′ E	428.4	1027	3,4,5,6,b
MSM33–53-1	**42° 05.01′ N**	**36° 37.37‘ E**	**443.4**	**797**	**a**
MSM33–52-1	42° 05.08′ N	36° 37.19‘ E	467.3	682	b
MSM33–61-1	42° 02.85′ N	36° 44.02‘ E	479.3	746	3,5,6,b
MSM33–60-1	41° 58.62′ N	36° 47.53‘ E	498.8	739	3,5,6,b
MSM33–64-1	42° 12.46′ N	36° 31.52′ E	660.5	721	3,4,5,6,b
MSM33–62-1	42° 13.15′ N	36° 30.11′ E	767.3	747	3,4,5,6,b
MSM33–63-1	42° 13.27′ N	36° 30.00′ E	785.5	704	3,4,5,6,b
M72/5–22GC3	42° 13.53′ N	36° 29.55′ E	838.0	839	1,2,5,6
M72/5–22GC4	**42° 13.54′ N**	**36° 29.53′ E**	**842.0**	**866**	**1,2,4,5,6,a**
M72/5–22GC6	42° 13.57′ N	36° 29.65′ E	843.0	800	1,2,4,5,6,b
M72/5–22GC8	42° 13.53′ N	36° 29.59′ E	847.0	945	1,2,4,5,6,b
GeoB7608–1	43° 29.2′ N	30° 11.8′ E	1202.0	685	a, c
GeoB7622–2	41° 32.1′ N	31° 10.1′ E	1305.0	565	a, d

(a) This study, (1) Nowaczyk *et al.* (2012), (2) Nowaczyk *et al.* (2013a), (3) Liu *et al.* (2018), (4) Nowaczyk *et al.* (2018), (5) Liu *et al.* (2019), (6) Liu *et al.* (2020), (b) Nowaczyk *et al.* (in prep), (c) Bahr *et al.* (2005), (d) Lamy *et al.* (2006).

and oxic water conditions, that is, the Black Sea was a freshwater lake. At around 8.2 ka, as a consequence of the global sea level rise associated with the last deglaciation, an ingression of marine seawater through the sill of the Bosporus (modern water depth 36 m) turned the Black Sea into the World's largest anoxic Basin (e.g. Major *et al.* 2006; Kwiecin *et al.* 2008). Since then, due to a persistent stratification, finely laminated organic-rich sapropelitic sediments and coccolith oozes were deposited (e.g. Bahr *et al.* 2005; Shumilovskikh *et al*. 2013). Further information is available from tephrochronological (e.g. Cullen *et al.* 2014) and palaeoclimatic studies (e.g. Wegwerth *et al*. 2014, 2015, 2016).

Core MSM33–53-1 was taken close to core M72/5–25GC1 (Fig. 1), which was recovered in 2007 from a water depth of 418.0 m during ship expedition M72/5 of German research vessel *RV Meteor*. Its data set will be compared to the new results from core MSM33–53-1 in the context of greigite contamination. During expedition M72/5 also core M72/5–22GC4 was recovered from a water depth of 842.0 m from the Arkhangelsky Ridge (Fig. 1). This is the only core from the two ship expeditions that was sampled by both discrete samples and U-channels. Greigite contamination in U-channel records will be discussed based on this data set.

2.2 XRF-logging

In order to obtain information about the distribution of the major elements, archive halves of split core MSM33–53-1 were used for down-core X-ray fluorescence (XRF) scanning at the Leibnitz Institute for Baltic Sea Research Warnemünde, Rostock, Germany. A COX Analytics ITRAX XRF Core Scanner (e.g. Croudace *et al.* 2006) was operated with a Cr-tube at 30 kV and 30 mA and a SDD Si drift detector, with an exposure time of 15 s and a step size of 1 mm. Data obtained from this method was mainly used for correlation purposes.

2.3 Palaeo- and rock magnetism

For correlation purposes also magnetic susceptibility was logged at 1 mm intervals applying a fully automated split-core logging system. Measurements were performed on the split-surface of core segments using a Bartington MS2E-1 spot-reading sensor. The sensor's response function with respect to a thin magnetic layer is a Gaussian curve with a half-width of a bit less than 4 mm, thus providing high-resolution logs of magnetic susceptibility. For palaeo- and rock magnetic purposes clear rectangular plastic boxes with a volume of 6 cm^3 (inner dimension 20 × 20 × 15 mm) were used. The depth interval in Core MSM33–53-1 between 332 and 597 cm, identified as MIS 3 by correlation with XRF records from other MSM33 cores, was sampled at high-resolution (Fig. 2). Two parallel rows of samples, with an offset of half a sample and all boxes being rotated by 45°, that is, with their diagonals being parallel to the core axis, yielded a resolution of 16–17 mm with a triangular weighting. Thus, a centre-weighting with only about 40 per cent overlap with the two neighbouring samples from the parallel row could be achieved (Fig. 2b). The remaining upper (younger) and lower (older) parts were sampled by pressing the boxes side-by-side into the core halves with their edges parallel to the core axis along a single row (Row 1 in Fig. 2c). This provides a rectangular (equal) weighting along the sampling interval. A second row with an offset of half a sample actually would not yield a higher resolution since the second row results in an overlap of about 70 per cent of one sample in row 1 with two adjacent samples from Row 2 (Fig. 2c). An AGICO Multifunction Kappabridge MFK1-A was then used to determine the low-field magnetic susceptibility κ_{LF}, and its anisotropy (AMS), of the samples.

The up to now unpublished palaeomagnetic record obtained from core M72–5/22GC4 based on U-channels will be discussed, too. Magnetostratigraphic results obtained from discrete samples of this core were published by Nowaczyk *et al*. (2012, 2013a). In core M72/5–22GC4, with a diameter of 12 cm, from 366 to 866 cm

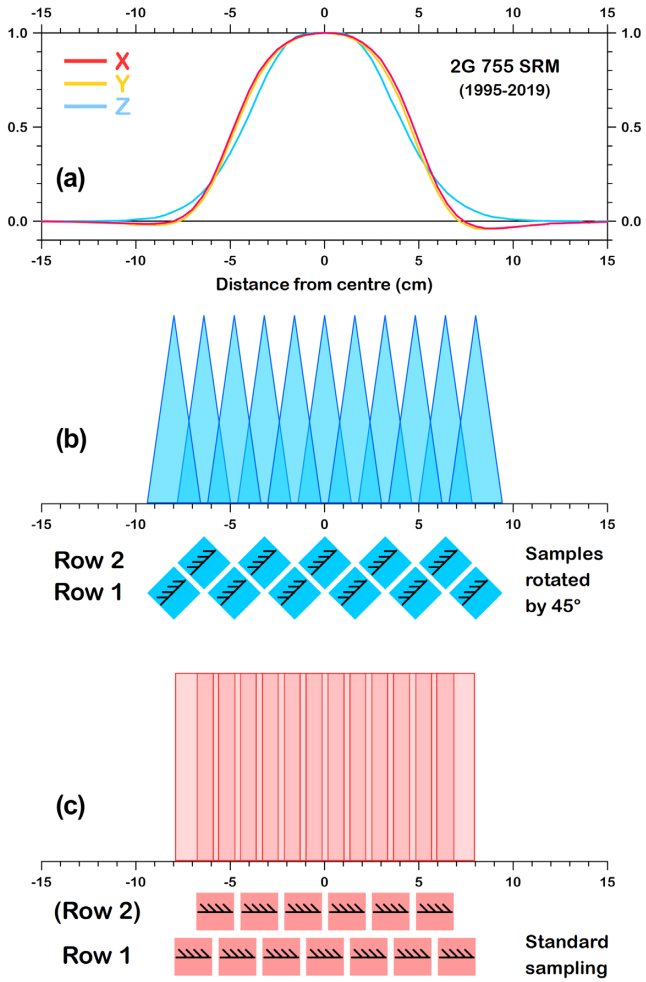

Figure 2. Comparison of three different measuring and sampling techniques, respectively, relevant for this study: (a) response functions of the three pick-up coils of the cryogenic long-core magnetometer used for U-channel measurements in this study, derived by moving a 2 mm small piece of basalt through the magnetometer, (b) spatial weighting functions of two parallel rows of cubic samples rotated by 45° against the core axis, (c) spacial weighting functions of two parallel rows of cubic samples in standard orientation, with their edges parallel to the core axis. The arrows on the samples are parallel to the samples' *Z*-axes. The darker shaded areas in the weighting functions in (b) and (c) indicate the overlap of one sample with two neighbouring samples in the parallel row. In (a) *X* and *Y* are the transverse components and *Z* is the axial component parallel to the long-core magnetometer's axis.

sub-bottom depth, 2 × 2 cm U-channels were taken parallel to discrete samples, mostly taken at high-resolution (Fig. 2b) as described before.

The natural remanent magnetization (NRM) of discrete samples and U-channels, as well as the anhysteretic remanent magnetization (ARM, discrete samples only) were measured with a 2G Enterprises 755 SRM (cryogenic) long-core magnetometer equipped with a sample holder for eight discrete samples at a separation of 20 cm. Measurements on U-channels were performed in steps of 1 cm extending 10 cm over both ends of the 1 m-long sediment profiles, yielding data sets spanning over 120 cm in total. These data sets, on basis of the measured Cartesian components (*X*, *Y*, *Z*), then were superimposed in order to compensate for the end-effect at the edges of the U-channels, thus yielding a continuous 500-cm-long palaeomagnetic record. The half-widths of the magnetometer's pick-up coils is about 9–10 cm, depending on component (Fig. 2a). Therefore, obtained U-channel data is not of high resolution.

The magnetometer's in-line tri-axial alternating field (AF) demagnetizer was used to demagnetize the NRM and ARM of the samples. The NRM was measured after application of AF peak amplitudes of 0, 5, 10, 15, 20, 30, 40, 50, 65, 80 and 100 mT. Directions of the characteristic remanent magnetization (ChRM) were determined by principal component analysis (PCA) according to Kirschvink (1980). The error range of the ChRM is given as the maximum angular deviation (MAD). The cores were not oriented in azimuth. Therefore, in order to obtain fully oriented directions, all declinations of a core were rotated to a common mean value of 0°. Declinations related to negative inclinations were shifted by 180° with their inclinations being multiplied by –1, that is, potential reversed directions were treated as normal directions. Averaging was then accomplished by applying Fisher (1953) statistics to all directions falling inside a circle of 35° around the expected dipole direction (D = 0°, I = 61°). Thus, transitional directions with, for example shallow inclinations and/or (after correction) easterly or westerly declinations, were not included in the calculation of the mean declination for the azimuthal correction.

The ARM was imparted along the discrete samples' *z*-axis with a static field of 0.05 mT and an AF field of 100 mT, using a separate single-axis 2G 600 AF demagnetizer. Demagnetization then was performed in steps of 0, 10, 20, 30, 40, 50, 65 and 80 mT. The median destructive field of the ARM (MDF_{ARM}) was determined to estimate the coercivity of the sediments. The slope of NRM versus ARM of common demagnetization steps was used to determine the relative palaeointensity (rPI). In most cases, demagnetization steps from 20 to 65 mT were used to determine the rPI. The ARM intensity normalized by the static field used to produce the ARM yields the anhysteretic susceptibility κ_{ARM}. Since the ARM mostly affects fine-grained particles, whereas the magnetic susceptibility κ_{LF} is influenced by all particles, high (low) values of the κ_{ARM}/κ_{LF} ratio indicates fine- (coarse-)grained particles.

A 2G Enterprises 660 pulse magnetizer was used to impart an isothermal remanent magnetization (IRM) along the discrete samples' *z*-axes. A peak field of 1.5 T was used to saturate the samples. The acquired magnetization is defined as the saturated IRM (SIRM). In order to avoid an over-ranging of the available cryogenic magnetometer, the samples' strong IRMs were measured with a Molyneux spinner magnetometer (noise level 0.2 mAm^{-1}). A backfield of –0.2 T (based on lab experience) was applied to each sample in order to determine the *S*-ratio, defined as 0.5 × [1-(IRM(-0.2 T)/SIRM)]. The *S*-ratio is close to 0 for pure haematite (Fe_2O_3) and close to 1 for both magnetite (Fe_3O_4) and greigite (Fe_3S_4). In order to be able to discriminate between the latter two minerals, the ratio of saturation magnetization over magnetic susceptibility SIRM/κ_{LF} was determined. Magnetite and greigite have similar SIRMs but the κ_{LF} of greigite is significantly lower than that of magnetite. Thus the presence of greigite can be indicated by SIRM/κ_{LF} ratios significantly higher than those for magnetite, especially in Black Sea sediments (Nowaczyk *et al.* 2012). Like for the κ_{ARM}/κ_{LF} ratio, high (low) values of the ARM/SIRM ratio indicate more fine- (coarse-)grained particles. All palaeo- and rock magnetic investigations on discrete samples and U-channels were performed at the Helmholtz Centre Potsdam, GFZ German Research Centre for Geosciences, Potsdam, Germany.

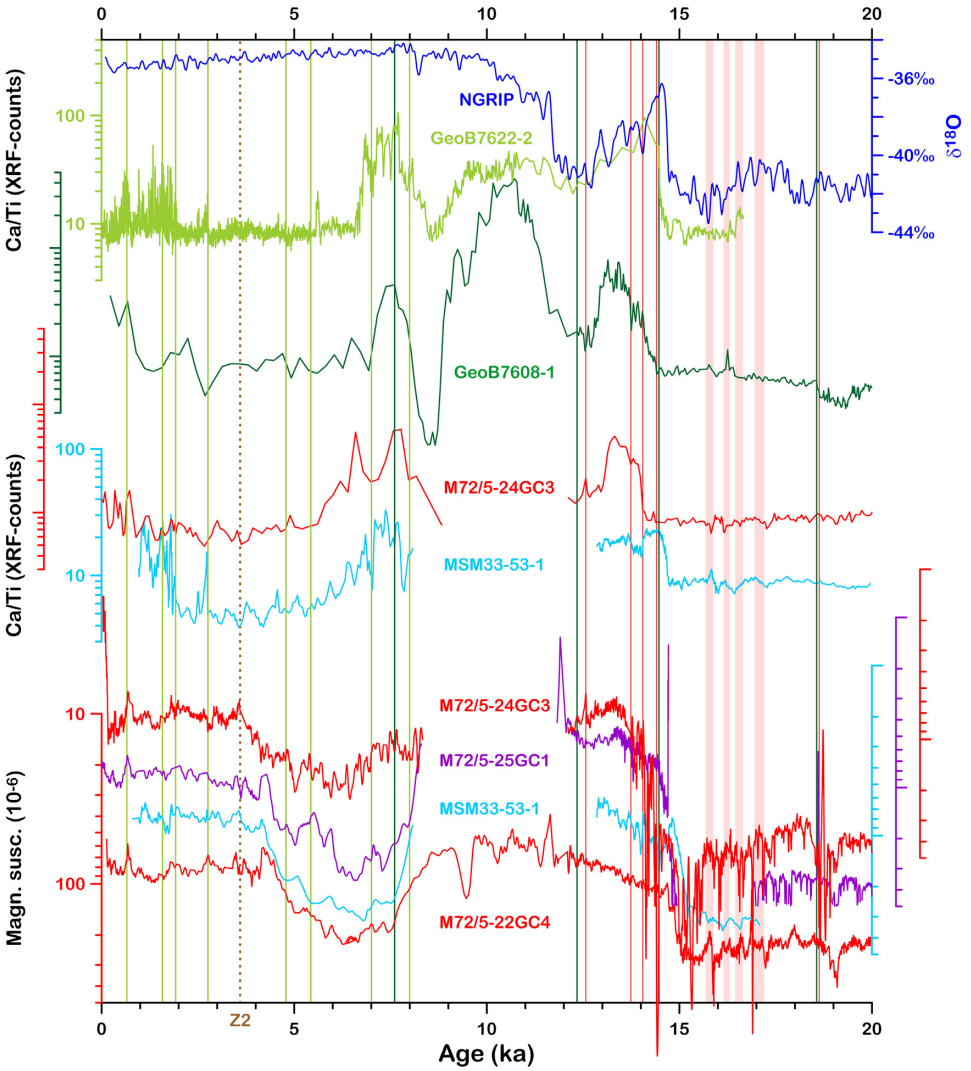

Figure 3. Age constraints for the studied cores from 0 to 20 ka. Oxygen isotope (δ^{18}O) record from Greenland ice cores (NGRIP, Svensson *et al.* 2008) together with XRF-derived Ca/Ti ratios and magnetic susceptibility logs from selected cores relevant for this study. Vertical solid lines mark AMS^{14}C ages from core GeoB 7622–2 (light green, Lamy *et al.* 2006), core GeoB7608–1 (dark green, Bahr *et al.* 2005), and core M72/5–24GC3 (red lines, Nowaczyk *et al.* 2012). The vertical dotted brown line at 3.6 ka marks the Z2 tephra from the Minoan eruption of Thera/Santorini (e.g. Höflmayer 2012), and vertical pink stripes mark the occurrence of AMS^{14}C-dated reddish layers at about 16 to 17 ka caused by meltwater events (Soulet *et al.* 2013; Liu *et al.* 2018).

3 RESULTS

3.1 Age models

For dating of investigated Holocene and late-glacial sediments from the SE Black Sea, accelerator mass spectrometry (AMS) ^{14}C ages from two cores recovered from the western Black Sea during *RV METEOR* cruise M51/4 in 2001 were adopted (Fig. 1, Table 1). Core GeoB7622–2 (Lamy *et al.* 2006) provides mainly ages for the Holocene back to about 8 ka (light green vertical lines in Fig. 3). Identification of the Z2 tephra layer related to the Minoan eruption of Thera/Santorini at around 1600 BCE (e.g. Höflmayer 2012) in core GeoB7622–2 (Lamy *et al.* 2006) and M72/5–25GC1 (Cullen *et al.* 2014) yielded a further tie point within the Holocene (brown dotted vertical line in Fig. 3). Core GeoB7608–1 (Bahr *et al.* 2005) provides AMS^{14}C ages from about 7.5 ka back to 27 ka (dark green vertical lines in Fig. 3), overlapping with AMS^{14}C ages from 12.5 ka back to 39.3 ka (red vertical lines in Fig. 3) from core M72/5–24GC3 (Nowaczyk *et al.* 2012). Four reddish sediment layers related to meltwater events during the decay of the Fennoscandian ice sheet, with AMS^{14}C-based ages from about 15 to 17 ka (pink vertical stripes in Fig. 3), described from the western Black Sea (Soulet *et al.* 2013), could also be found in the SE Black Sea. Here, they were identified best from their maxima in K/Ti ratios as well as by their minima in S-ratios, reflecting an increased haematite content that causes the visible reddish hues of the corresponding sediments (Liu *et al.* 2018). Further-on, detailed counting of ice-rafted debris (IRD, 'drop-stones') on cores M72/5–22GC8, M72/5–24GC3, and M72/5–25GC1 (Nowaczyk *et al.* 2012, 2013a) yielded a clear pattern of warming/cooling cycles that could be unequivocally correlated to the sequence of 'Dansgaard-Oeschger' (DO) warming events (Dansgaard *et al.* 1993) defined from Greenland ice core oxygen isotope stratigraphy (Svensson *et al.* 2008). These results provided mainly age constraints from about 25 to 69 ka (DO events 3 to 18, see Fig. 4). These heterogeneous age constraints

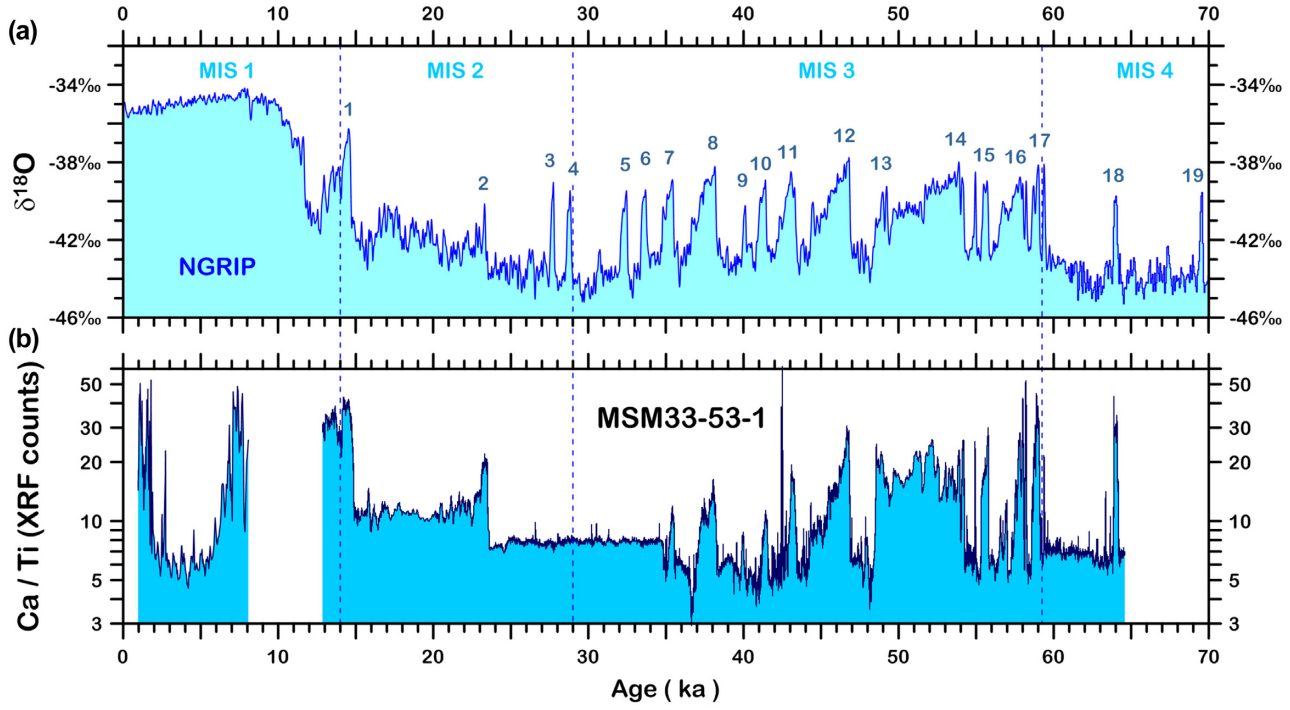

Figure 4. Age constraints for core MSM33–53-1 for ages older than about 35 ka: (a) Oxygen isotope ($\delta^{18}O$) record from Greenland ice cores (NGRIP, Svensson *et al.* 2008) and (b) Ca/Ti ratio from XRF-scanning of core MSM33–53-1 after correlation to NGRIP. In (a) numbers from 1 to 19 refer to the Dansgaard-Oeschger events (Dansgaard *et al.* 1993). Vertical dashed lines indicate the boundaries of the marine isotope stages (MIS).

were transferred to all other cores from the SE Black Sea that were studied for palaeomagnetism (Table 1). A multiple-parameter correlation, mainly based on high-resolution magnetic susceptibility and element ratios (Ca/Ti, K/Ti) obtained from XRF scanning, and, last but not least, palaeomagnetic results, then yielded age models with a minimum of discrepancies and/or ambiguities. For example, following the AMS^{14}C ages from cores GeoB7608–1 (dark green) and core M72/5–24GC3 (red) at around 14.5 ka (Fig. 3), the obtained correlation leaves some ambiguities in the range of a few hundred years. In any case, correlation of magnetic susceptibility and Ca/Ti ratios to the oxygen isotope record from Greenland especially from the end of the last glacial on is not straightforward (Fig. 3). This is mainly due to the change from a freshwater/brackish regime into full marine conditions at around 8.2 ka, associated with a significant drop and a subsequent rise in the Ca/Ti ratio, but a temporal increase in susceptibility, which is generally lower in the Holocene when compared to the glacial (note the inverted axes in Fig. 3).

From the correlation procedure it became obvious that several cores are affected by a hiatus from about 8.0 to 12.5 ka (e.g. M72/5–24GC3, M72/5–25GC1, MSM33–53-1; Fig. 3). The sequence of DO events is only partly seen in the Ca/Ti ratio from XRF scanning in core MSM33–53-1. The correlation of Ca/Ti ratio from this core to the NGRIP oxygen isotope record is shown in Fig. 4. In the interval from 23.5 ka to about 34 ka the Ca/Ti ratio is unusually flat, whereas older sediments show a clear correlation to NGRIP. This probably indicates a homogenized interval due to a slump. However, this is not relevant for the interpretation of palaeomagnetic data of the Laschamps excursion occurring at 41 ka. Further age tie points were provided by identification of two tephra layers in glacial sediments. The cape Riva eruption of Santorini at 21.8 ± 0.4-ka (Fabbro *et al.* 2013) is related to the Y2 tephra. The Y5, or Campanian Ignimbrite tephra is related to the big eruption of the Phlegrean Fields (De Vivo *et al.* 2001; Pyle *et al.* 2006). Its new calibated AMS ^{14}C age of 39.85 ± 0.14 ka (Giaccio *et al.* 2017) confirms its close stratigraphical position shortly after the Laschamps excursion centred at 41 ka as found by Nowaczyk *et al.* (2012). Obtained age models of all Black Sea cores relevant for this study are shown in Fig. 5, back until 70 ka. Obviously, for most of the coring sites in the SE Black Sea, the end of the last glacial lead to a dramatic decrease in sedimentation rates from about 50 cm ka^{-1} in MIS 2 down to only 5 to 10 cm ka^{-1} in MIS 1. MIS 3 is mostly characterized by sedimentation rates from 20 to 30 cm ka^{-1}, with lowest values in early MIS 3, characterized by generally higher temperatures and longer warm phases (DO events 12–17), while glacial erosion onshore in the preceding MIS 4 led to higher sedimentation rates. Also some hiatuses could be detected. These gaps in the sedimentary sequences at the slope of the Akchangelsky Ridge (Fig. 1) are interpreted as the effect of slumping down of sediments mobilized by the tectonic (earthquake) activity in this region.

3.2 Magnetostratigraphy of core MSM33-53-1

The typical approach to remove viscous overprints is to stepwise demagnetize samples with alternating fields (AF) of increasing peak-amplitude. Samples carrying a reversed magnetization need amplitudes of at least 20 mT to partly even 50 mT (e.g. Nowaczyk *et al.* 2003) in order to completely remove the normal polarity overprint. Normally, the remaining NRM then is demagnetized in further steps of up to 100 mT peak AF amplitude in order to provide the data base for principal component analysis for determining the ChRM direction. In many cases of a NRM partly or mostly carried by greigite the acquisition of a gyro-remanent magnetization (GRM) occurs at

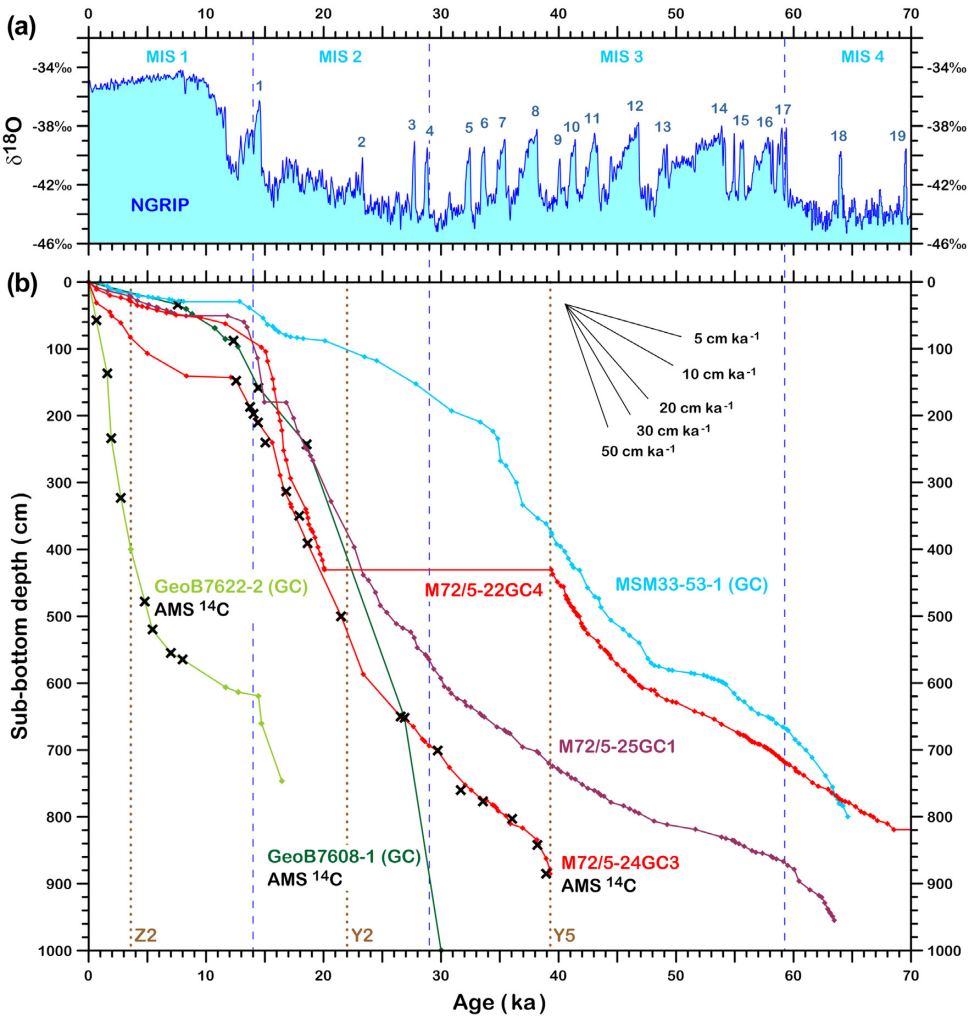

Figure 5. Age models of the sediment cores from the Black Sea discussed in this paper in the context of the palaeoclimatic history: (a) Oxygen isotope (δ^{18}O) record from Greenland ice cores (Svensson *et al.* 2008) and (b) depth-age-relationships of the cores with indications for sedimentation rates by the bunch of lines in the top of (b). The position of tephra layers are indicated by vertical brown dotted lines. Z2–Minoan tephra (e.g. Höflmayer 2012), Y2–Cape Riva tephra (e.g. Fabbro *et al.* 2013), Y5–Campanian Ignimbrite tephra (e.g. Giaccio *et al.* 2017). Vertical dashed lines indicate the boundaries of the marine isotope stages (MIS).

these steps (e.g. Snowball 1997; Roberts *et al*. 2011). GRM acquisition visibly starts at peak AF fields of about 40–65 mT (e.g. Ron *et al.* 2007), mostly acquired perpendicular to the last axis that was demagnetized. Thus, demagnetization data, needed for determining the ChRM direction by PCA analysis, can get compromised by the GRM acquisition in greigite. As a case study for such a conflict between the need to go to higher peak fields to isolate the ChRM direction, on the one hand, and the acquisition of artificial GRMs at these steps, on the other hand, results from core MSM33–53-1 shall be discussed here in detail.

Fig. 6 shows AF demagnetization data as vector endpoint diagrams from eight samples from core MSM33–53-1. The demagnetization data is plotted together with down-core palaeo- and rock magnetic data from between 370 and 460 cm: relative palaeointensity (slope (NRM/ARM)), ChRM declination and inclination, and the greigite-indicative SIRM/κ_{LF} ratio. Like in four parallel cores of expedition M72/5 from Site 22 (Fig. 1), the Laschamps excursion, centred at 41 ka (Nowaczyk *et al.* 2012), is identified from steep negative inclinations and declinations around 180° from about 400 to 430 cm. Obviously, AF demagnetization results from across the Laschamps excursion is affected by greigite present in the sediments, indicated by frequent SIRM/κ_{LF} ratios >10 kAm^{-1}. This is also expressed by some GRM-acquisition throughout AF demagnetization of these samples, that is, vector endpoints at the highest AF levels do not really migrate straight to the origin of the diagrams anymore (Fig. 6). Therefore, during PCA analysis of the AF results, for each sample, tentatively, an interval of at least three successive demagnetization steps was picked where the adjusted line points towards the origin of the diagram. In Fig. 6 these steps are marked in black.

The complete down-core plot of data obtained from core MSM33–53-1 is shown in Fig. 7. In the left-hand panel, the NRM (black) and ARM (green) intensities are plotted together with the estimate of relative palaeointensity as derived from the slope of NRM versus ARM of common demagnetization steps. In the middle panel of Fig. 7 ChRM inclinations and declinations are displayed with various filter levels as discussed further down. The blue bar marks the interval of high-resolution sampling (Fig. 2b). The down-core

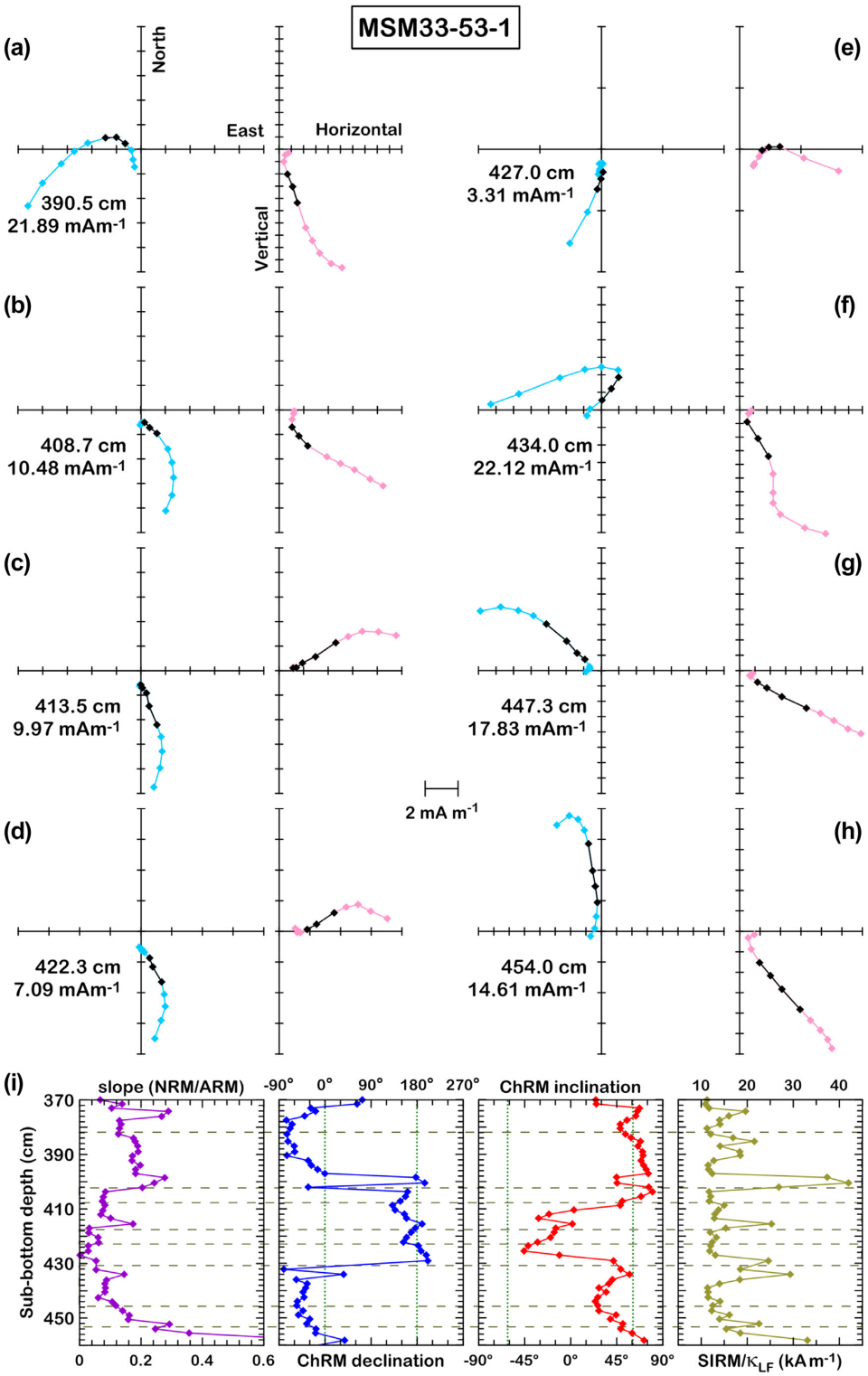

Figure 6. Results from alternating field demagnetization of eight samples from core MSM33–53-1 across the Laschamps excursion shown as separately scaled vector end point diagrams (a–h). The variation in declination (inclination) is shown in the left (right) diagram by blue (pink) diamonds. The distance between two ticks is equivalent to 2 mAm^{-1}. Explicit values given in mAm^{-1} denote the samples' NRM intensities. The stratigraphic positions of the eight samples are marked by horizontal dashed lines in the down-core plots from 370 to 460 cm (f) of slope (NRM/ARM), as the proxy for relative palaeointensity, ChRM declination and inclination, and the rock magnetic parameter $SIRM/k_{LF}$, with values >10 kAm^{-1} indicating the presence of greigite. NRM—natural remanent magnetization, ARM—anhysteretic remanent magnetization, ChRM—characteristic remanent magnetization, SIRM—saturated iso-thermal remanent magnetization, κ_{LF}—low field magnetic volume susceptibility.

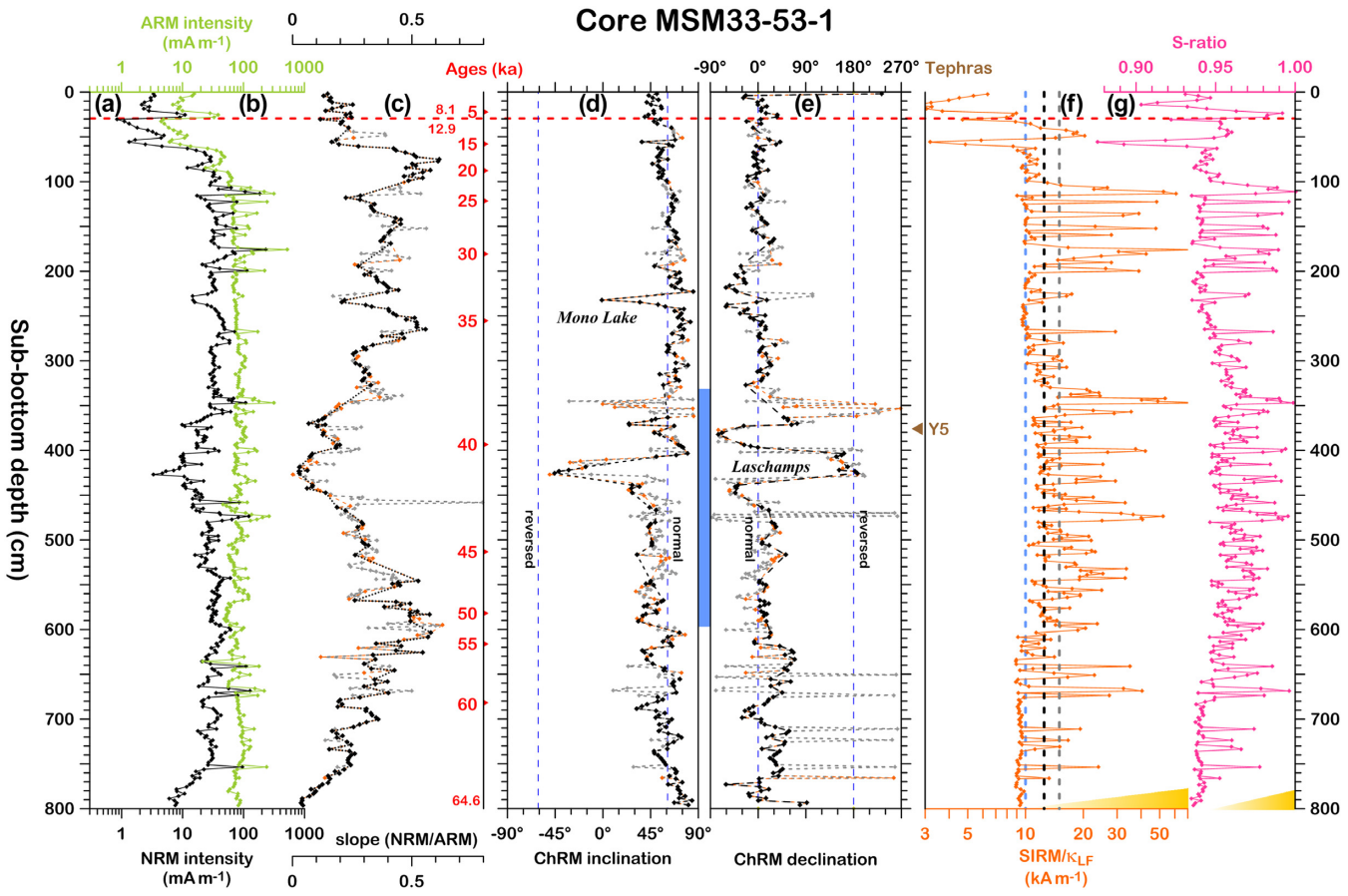

Figure 7. Down-core plots of palaeo- and rock magnetic results from core MSM33–53-1: (a) NRM intensity, (b) ARM intensity, (c) relative palaeointensity estimated from the slope of NRM versus ARM intensity of common demagnetization steps, (d) ChRM inclination and (e) declination, (f) SIRM/k_{LF}, as a proxy for the presence of greigite, and (g) S-ratio, with lower (higher) values indicating increasing haematite (greigite) content. Ages are given by red numbers in (c). The position of the Y5 (Campanian Ignimbrite tephra, e.g. Giaccio *et al.* 2017) is marked in (f). Yellow triangles in (f) and (g) indicate increasing greigite content. The horizontal red dashed line indicates the position of a major hiatus. Vertical blue dashed lines in (d) and (e) mark the direction expected from a geocentric axial dipole for normal and reversed polarity, respectively. Unfiltered palaeomagnetic data in (c–e) is shown in orange colour. Different levels for the exclusion of palaeomagnetic data are shown in black and grey colours according to their threshold values (vertical dashed lines in f), see Section 3.2. The blue bar between (d) and (e) marks the depth interval sampled at high-resolution (see Fig. 2b). NRM—natural remanent magnetization, ARM—anhysteretic remanent magnetization, ChRM—characteristic remanent magnetization, SIRM—saturated iso-thermal remanent magnetization, k_{LF}—low field magnetic volume susceptibility, *S*-ratio—definition see Section 2.3.

variations of the S-ratio and the SIRM/κ_{LF} ratio are plotted in the right panel. For filtering out greigite-bearing samples from Black Sea sediments, Nowaczyk *et al*. (2012, 2013a) defined a SIRM/κ_{LF} ratio threshold level of 10.0 kAm^{-1}, with samples below (above) 10 kAm^{-1} being free of (increasingly contaminated by) greigite. This threshold level is marked by a vertical dashed blue line in the down-core plot of the SIRM/κ_{LF} ratio (Fig. 7f). Applying this strict criterion (SIRM/κ_{LF} > 10 kAm^{-1}) would eliminate every sample between 300 and 600 cm, including the clearly expressed record of the Laschamps excursion. Therefore, in order to check the performance of less restrictive criteria, threshold levels of 12.5 and 15.0 kAm^{-1} were applied to the data. Unfiltered directional palaeomagnetic data, slope (NRM/ARM), ChRM inclinations and declination, are plotted in orange (Figs 7c-e). Cutting off data with SIRM/κ_{LF} ratios above 15.0 kAm^{-1} (grey dashed line, Fig. 7f) excludes many of greigite-related spikes in the palaeomagnetic data, but still some anomalous data points are left, for example at around 350 cm (grey symbols, Figs 7c–e). The filter level of 15.0 kAm^{-1} leaves 252 out of 369 samples, or 68.3 per cent of the data. Using the 12.5 kAm^{-1} threshold (black dashed line, Fig. 7f) results in a fairly consistent palaeomagnetic record (black symbols, Figs 7c–e), though now only 200 out of 369 samples are left, equal to just 54.2 per cent of the whole data. Nevertheless, this filtered palaeomagnetic record from core MSM33–53-1 provides evidence for the Mono Lake excursion (Denham & Cox 1971; Liddicoat & Coe 1979; Lund *et al.* 1988; Channell 2006; Cassata *et al.* 2010; Kissel *et al.* 2011, Liu *et al.* 2019) at 34.5 and the already mentioned Laschamps excursion centred at 41.0 ka. Partly, some filtered out data points seem to fit into the remaining data, such as between 530 and 545 cm depth, where SIRM/k_{LF} ratios are around 20 kAm^{-1}, and more. Thus, gaps in the records of inclination, declination, and relative palaeointensity might be closed, but no clear criteria could be defined how to discriminate between these points and points which are definitely outliers. Moreover, often only in one or two of the three records (rPI, inclination, declination) gaps can be closed.

3.3 Magnetostratigraphy of core M72/5-25GC1

As can be seen in Fig. 1, cores MSM33–53-1 and M72/5–25GC1 have been recovered from nearby sites (see also Table 1). Therefore, the palaeomagnetic records from both cores suffer in a similar

way from severe greigite contamination (compare Figs 7 and 8). Magnetite-bearing samples in core M72/5–25GC1 can be better separated from greigite-bearing samples (Figs 8f and g). But, by filtering out samples with SIRM/k_{LF} ratios > 10 kAm-1, only about 25 per cent of investigated samples remain. Also in core M72/5–25GC1 a record of the Laschamps excursion is documented at a depth of around 750 cm, almost twice the depth of the Laschamps excursion in core MSM33–53-1. This is likely due to small-scale bathymetric modulation along the slope of the Arkhangelsky Ridge, not visible in Fig. 1, causing local variations in sedimentation rates (Fig. 5). Though resampled at high resolution (blue bar in Fig. 8), the record of the Laschamps excursion seems to be problematic. Inclinations do not reach steep negative inclinations, such as in other cores from that area, like in core M72/5–22GC4 (Fig. 9, see also Nowaczyk *et al.* 2012; Liu *et al.* 2020), and declinations after the termination of the Laschamps excursion fluctuate around 180°, neither seen in core MSM33–53-1 (Fig. 7), nor in core M72/5–22GC4 (Fig. 9), discussed further down. Also at around 57 ka obviously anomalous declinations around 180°, not seen in other cores, were recorded in core M72/5–25GC1. Therefore, the palaeomagnetic record from core M72/5–25GC1 older than 40 ka was not considered for stacking of palaeomagnetic data from the SE Black Sea (Nowaczyk *et al*. 2012, 2013a; Liu *et al.* 2020).

3.4 Magnetostratigraphy of core M72/5-22GC4

The palaeo- and rock magnetic record from core M72/5–22GC4, but only the interval from 350 to 860 cm, is shown in Fig. 9. The full palaeo- and rock magnetic data set based on discrete samples from this core was already published in Nowaczyk *et al*. (2012, 2013a). Hitherto unpublished NRM intensity and ChRM directions obtained from U-channel measurements are shown by bolt light blue lines, whereas palaeomagnetic results from discrete samples with SIRM/k_{LF} ratios $\leq$ (>) 10 kAm^{-1} are marked by black (orange) diamonds. Rock magnetic results, SIRM/k_{LF} and *S*-ratio, were only determined on discrete samples (Figs 9f and g). The palaeomagnetic record from core M72/5–22GC4, recovered from a much deeper site (842.0 m) than cores MSM33–53-1 (443.4 m) and M72/5–25GC1 (418.0 m, see also Fig. 1, Table 1), is much less affected by the presence of greigite (Figs 9f and g). According to this, only a few samples had to be excluded from the palaeomagnetic record from discrete samples (orange diamonds, Figs 9d and e). Also in core M72/5–22GC4 the interval around the Laschamps excursion, identified in advance by correlation with other cores from site M72/5–22 (Fig. 1), was sampled at high resolution (Fig. 2b, blue vertical bar in Fig. 9), with data points every about 16 mm. U-channel data is plotted as light blue curves behind the discrete sample data. Dark green dashed horizontal lines mark the U-channel (section) breaks in Fig. 9. The U-channel data was acquired with low-resolution sensors (half-widths 9–10 cm, Fig. 2a). Therefore, in general, the low-pass filtered curves do not peek out from behind the discrete sample records, plotted as black diamonds in Fig. 9. But, there are some intervals, marked by yellow arrows in the NRM record, where the intensity in the U-channel record is much higher than in the discrete sample record (Fig. 9a). In the same intervals also inclination (Fig. 9d) and declination (Fig. 9e) show anomalous values. This is due to greigite-bearing intervals identified from GRM acquisition. Apparently, in the discrete sample data there is little evidence for this from the greigite-indicative SIRM/k_{LF} ratio (Fig. 9f). But, in the studied Black Sea sediments, greigite is mostly not present as continuous layers but more in non-stratiform spots, nodules, or concretions, only some millimetres to a few centimetres in size. Thus, it is possible to sample a greigite-bearing portion of sediment by the U-channel and not by discrete samples, and vice versa. Due to the wide sensor characteristics of the magnetometer, by comparison with the high-resolution discrete sample data, any small greigite nodule can spoil an interval of about 15 cm in the U-channel record that finally has to be cut out from the record. 15 cm is about 1.5 times the half-width of the magnetometer's sensors. Thus, even data obtained with a high-resolution magnetometer (half-width 5 cm), would be still spoiled over 7–8 cm. In contrast to this, the applied high-resolution sampling (Fig. 2b) by discrete samples (every 1.6 cm) would lose probably just one data point.

Luckily, the whole Laschamps excursion recorded in core M72/5–22GC4 between 380 and 480 cm depth is almost unaffected by the presence of greigite. In this interval only three samples had to be filtered out. But, in the U-channel data, the terminating westerly swing in declination between 425 and 445 cm depth (∼39 ka) is characterized by completely anomalous data (Figs 9a, d and e). The declination spike at the onset of the totally reversed phase at 490 cm depth (Fig. 9e) is associated with steep inclinations of almost -90° (Fig. 9d), where declinations can show very large variability. Thus, it is nothing erratic. Unlike in cores MSM33–53-1 (Fig. 7) and M72/5–25GC1 (Fig. 8), due to a hiatus, the Mono Lake excursion is not present in the sediments recovered from site M72/5–22. Very likely, an earthquake at about 20 ka triggered a submarine landslide at the Arkhangelsky Ridge, erasing all sediments that had been deposited until that point in time since about 39 ka (Fig. 4). Probably, the loose ash particles of the Y5 (Campanian Ignimbrite) tephra layer (see Fig. 5) acted as a weak link between these sticky clayish sediments and underlying deposits with a similar consistency that did not slide down the slope.

4 DISCUSSION

ChRM directions from core MSM33–53-1 and M72/5–22GC4, from the time interval from 42.5 to 39.4 ka, bracketing the Laschamps excursion, were transformed into virtual geomagnetic pole (VGP) positions (Fig. 10). 90°-rotated Hammer-Aitoff (equal area) projections, with the geographic poles centred in the respective hemispheres, are used for discussion. The advantage of this projection, in comparison to the more common equatorial Hammer-Aitoff projection, is that VGP movements at northern or southern high latitudes are projected with minimum distortion and, what might be even more important, without a break in longitude. VGPs from discrete sample data (closed diamonds) and U-channel data (open diamonds) from core M72/5–22GC4 (Fig. 10b) are compared with the VGP path of the stack based on discrete samples from all four cores from site M72/5–22 (Fig. 1, Table 1), investigated for palaeomagnetism (Nowaczyk *et al.* 2012). Individual VGP positions from the four cores from site M72/5–22 are shown as coloured closed diamonds (Fig. 10a) while the corresponding stack is shown as a black bold dotted line in all three projections of Fig. 10. Since core M72/5–22GC4 is included in the stack its VGPs are aligned with the VGP path of the stack. But, this is only valid for the discrete sample data (blue closed diamonds), while there is an eastward longitudinal offset of around 30° between the U-channel data (light blue solid line) and the stack visible for the N-R transition of the Laschamps polarity excursion (Fig. 10b) between about 41.5 and 41.1 ka. Symbols in the U-channel-related VGP path (Fig. 10b; open blue diamonds) are related to ChRM directions determined in 1 cm steps. The VGP

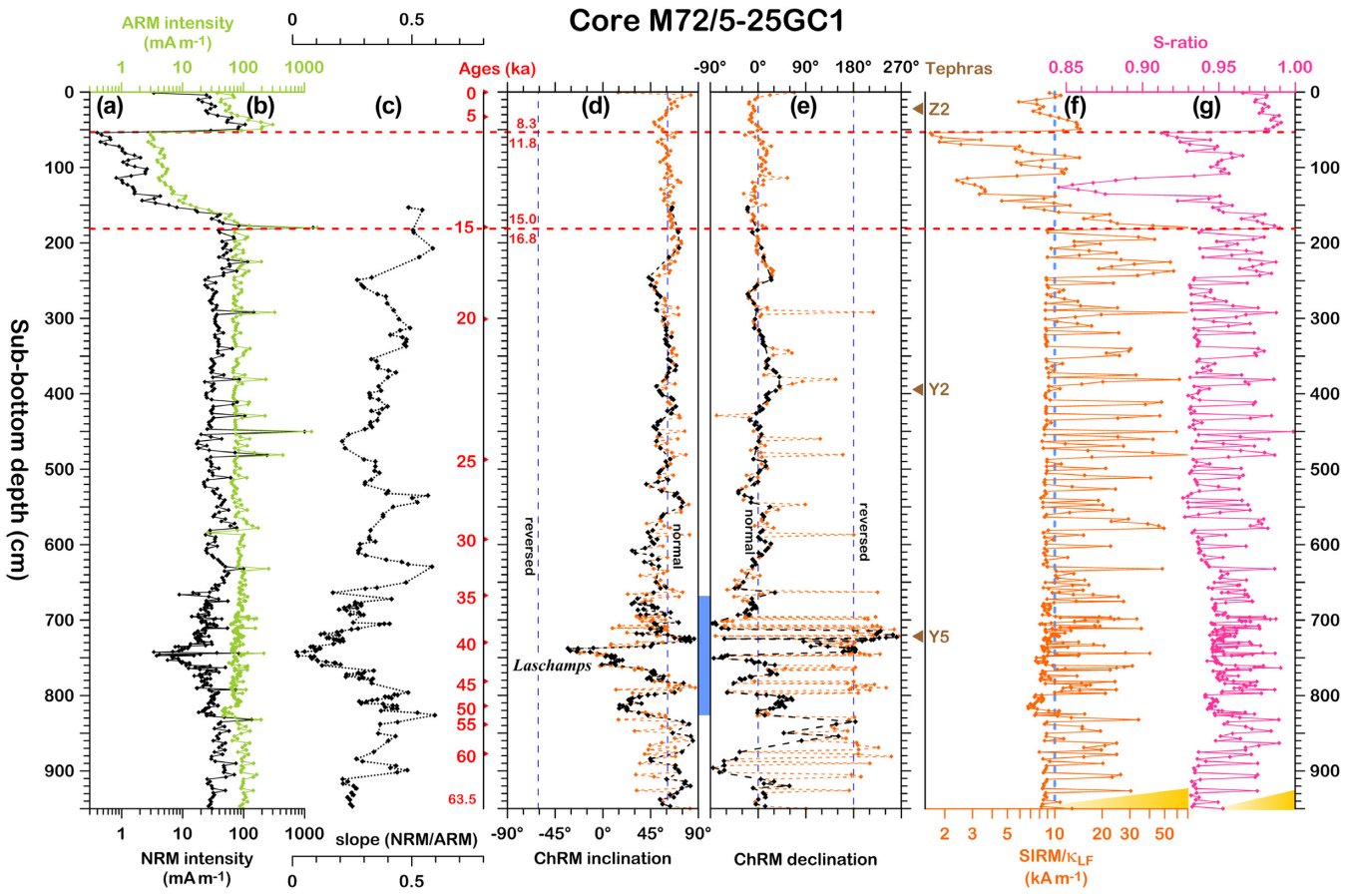

Figure 8. Down-core plots of palaeo- and rock magnetic results from core M72/5–25GC1: (a) NRM intensity, (b) ARM intensity, (c) relative palaeointensity estimated from the slope of NRM versus ARM intensity of common demagnetization steps, (d) ChRM inclination and (e) declination, (f) SIRM/k_{LF}, as a proxy for the presence of greigite and (g) *S*-ratio, with lower (higher) values indicating increasing haematite (greigite) content. Ages are given by red numbers in (c). The position of the tephra layers are marked in (f). Yellow triangles in (f) and (g) indicate increasing greigite content. The horizontal red dashed lines indicate the positions of major hiatuses. Vertical blue dashed lines in (d) and (e) mark the direction expected from a geocentric axial dipole for normal and reversed polarity, respectively. The vertical dashed line in (f) marks the threshold level for the exclusion of palaeomagnetic data (c, d, e; see Section 3.3). The blue bar between (d) and (e) marks the depth interval sampled at high-resolution (see Fig. 2b). NRM—natural remanent magnetization, ARM—anhysteretic remanent magnetization, ChRM—characteristic remanent magnetization, SIRM—saturated iso-thermal remanent magnetization, k_{LF}—low field magnetic volume susceptibility, *S*-ratio—definition see Section 2.3.

path section showing the offset, therefore, is related to a depth interval of only 10 cm. This is about equivalent with the half-widths of the magnetometers' pick-up coils (Fig. 2a). These wide sensor characteristics have a significant smoothing effect, which result in divergencies from high-resolution data of short-term geomagnetic field behaviour. The discussed interval of 10 cm is equivalent to about 400 yr, according to a mean sedimentation rate of 25 cm ka^{-1} in this interval (see Fig. 5). Though the smooth VGP path obtained from U-channels looks more appealing than the VGP stack from discrete samples, it is biased by the low-pass filtering of the magnetometer. The used magnetometer was installed in Potsdam in 1995, about the time when high-resolution long-core magnetometers were invented (Weeks *et al.* 1993). But since the main focus was set on discrete samples then, due to their higher flexibility in sampling and processing, a magnetometer with wide sensor characteristics having a constant response over 2 cm (standard sample size; compare Figs 2a and c) was preferred. According to the study of Philippe *et al.* (2018), comparing data from artificial discrete samples and U-channels, even narrow response functions introduce directional artefacts and suppress short-term excursional features in a palaeomagnetic record. Philippe *et al.* (2018) even concluded 'that the U-channel measurement technique is not appropriate for extracting significant information about detailed field morphologies during reversals and excursions and that such records should be systematically accompanied by discrete samples'. This relates mostly to regimes with low(er) sedimentation rates, but in the case of the present study with the Laschamps excursion recorded with 25 cm ka^{-1} similar effects can be observed, though measured with a low-pass filtering magnetometer.

The latitudinal offset in VGP positions between U-channel and discrete sample data in the N-R transition could also be due to some greigite, carrying an anomalous direction. In the record of the discrete sample there is evidence for the presence of greigite in this depth interval (Fig. 8f). Greigite was also the reason why the last phase of the Laschamps polarity excursion, the swing back from a westerly excursion in declination, VGPs younger than 39.8 ka (Fig. 10b), is almost completely distorted (Fig. 9e) and, therefore, was not be transferred into VGP positions. In any case, this late phase of the Laschamps excursion is a bit cut off due to the hiatus from ~39.4 to 20.0 ka, present in all site M72/5–22 cores. An

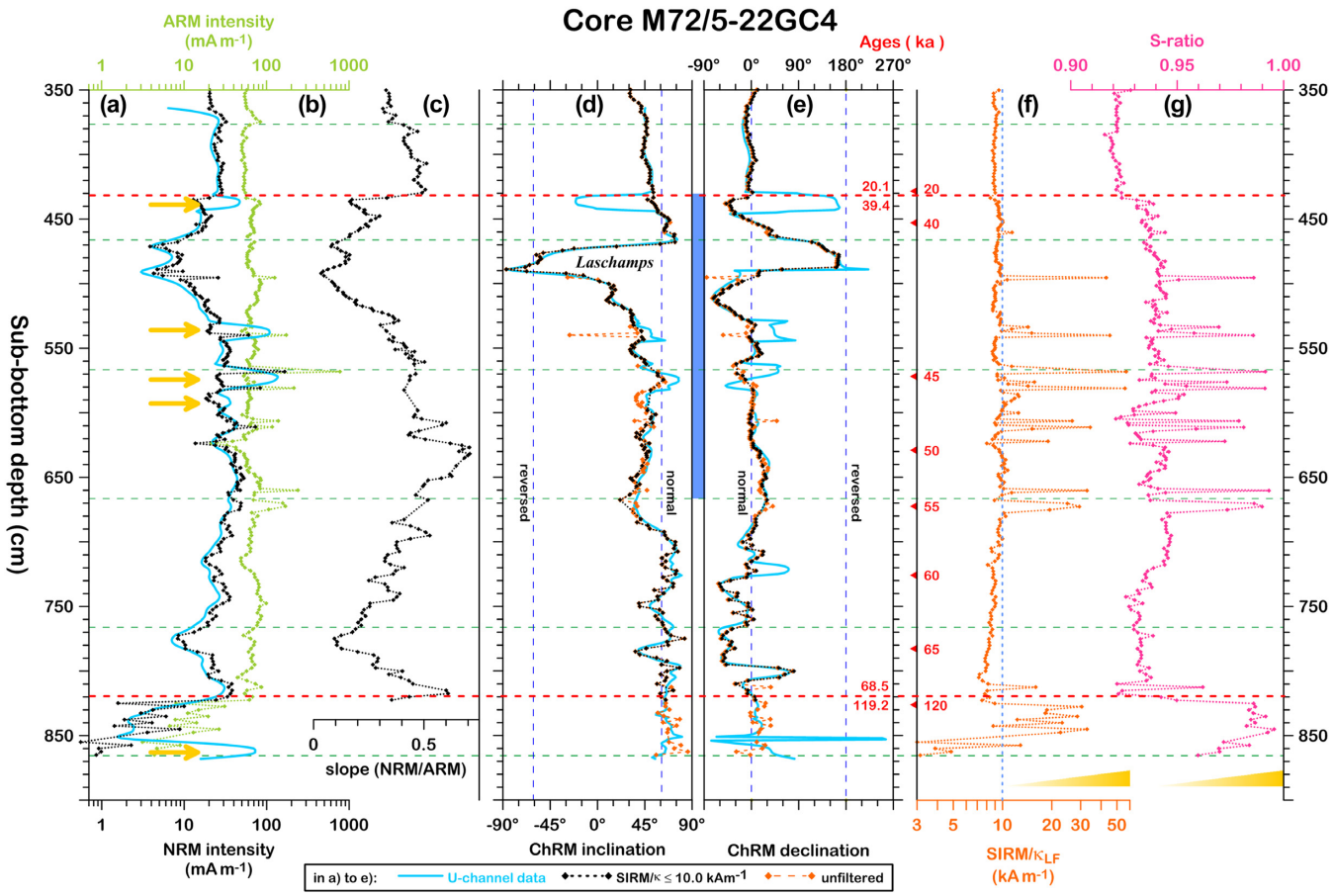

Figure 9. Down-core plots of palaeo- and rock magnetic results from core M72/5–22GC4: (a) NRM intensity, (b) ARM intensity, (c) relative palaeointensity estimated from the slope of NRM versus ARM intensity of common demagnetization steps, (d) ChRM inclination and (e) declination, (f) SIRM/k_{LF}, as a proxy for the presence of greigite, and (g) *S*-ratio, with lower (higher) values indicating increasing haematite (greigite) content. The results from U-channel measurements are shown by light blue curves (a, d, e). Ages are given by red numbers in (f). Yellow arrows in (a) mark the intervals biased by erratic remanences carried of greigite in the U-channel record. Yellow triangles in (f) and (g) indicate increasing greigite content as derived from discrete samples. The horizontal red dashed lines indicate the positions of major hiatuses. Horizontal green dashed lines indicate section breaks. Vertical blue dashed lines in (d) and (e) mark the direction expected from a geocentric axial dipole for normal and reversed polarity, respectively. The vertical dashed blue line in (f) marks the threshold level for the exclusion of palaeomagnetic data (c, d, e; see Section 3.4). The blue bar between (d) and (e) marks the depth interval sampled at high-resolution (see Fig. 2b). NRM—natural remanent magnetization, ARM—anhysteretic remanent magnetization, ChRM—characteristic remanent magnetization, SIRM—saturated iso-thermal remanent magnetization, k_{LF}—low field magnetic volume susceptibility, *S*-ratio—definition see Section 2.3.

uninterrupted record of this feature is better seen, though in lower resolution, in the data from core MSM33–53-1, at around 380 cm depth (Figs 6i and 7e).

VGP data derived from core MSM33–53-1 from unfiltered data (small orange filled diamonds), from samples with SIRM/$k_{LF} \leq 15.0$ kAm^{-1} (black open diamonds), and from samples with SIRM/$k_{LF} \leq 12.5$ kAm^{-1} are shown in Fig. 10c (black filled diamonds). The onset of the Laschamps excursion, the movement of VGPs from northern North America to the Caribbean is partly recorded (Fig. 10c). But then VGPs migrate directly from the Caribbean to Antarctica. Thus, the complete track of the N-R transition of the Laschamps excursion towards Antarctica is missing, likely due to a short-term hiatus in the range of a few hundred years. Due to the great circle connection, the shortest path, between VGP positions at about 41.8 and 41.04 ka (Fig. 10c), apparently the VGPs took a path different from the stack. The R-N transition from Antarctica to Central Siberia follow more or less the track of the VGP stack obtained from site M72/5–22. Also the last swing towards southerly VGPs at about 39.8 ka and then back to northern high latitudes at 39.4 ka is recorded in MSM33–53-1 (compare Figs 10b and c). This description is based on VGPs from samples with SIRM/$k_{LF} \leq 12.5$ kAm^{-1}. Partly, gaps of this track can be filled in by VGPs from samples with SIRM/$k_{LF} \leq 15.0$ kAm^{-1} (open black diamonds; Fig. 10c). Thus, at least for the discussed time interval, the less strict filter criterion of SIRM/$k_{LF} \leq 15.0$ kAm^{-1} would have provided a fairly trustful record. Also a few VGP positions from unfiltered samples in the MSM33–53-1 data (Fig. 10c, small orange filled diamonds) fit to the VGP path of the Black sea stack, but the majority don't. Thus, samples with their remanence influenced, or dominated by greigite did not provide correct palaeomagnetic data.

Time series of the Laschamps excursion obtained from Black Sea sediments from the time interval 44 to 38 ka are summarized in Fig. 11. Inclinations (Fig. 11a), declinations (Fig. 11b), and relative palaeointensities (Fig. 11c) are compiled from cores M72/5–25GC1 and MSM33–53-1 (left-hand panel), M72/5–22GC4, with separate data from U-channels and discrete samples (right-hand panel) and the stack from site M72/5–22 (middle panel). Cores M72/5–25GC1 and MSM33–53-1 are the only cores from the Arkhangelsky Ridge providing an uninterrupted record of the Laschamps excursion. Unfortunately, their data sets are fragmentary due to the necessity of

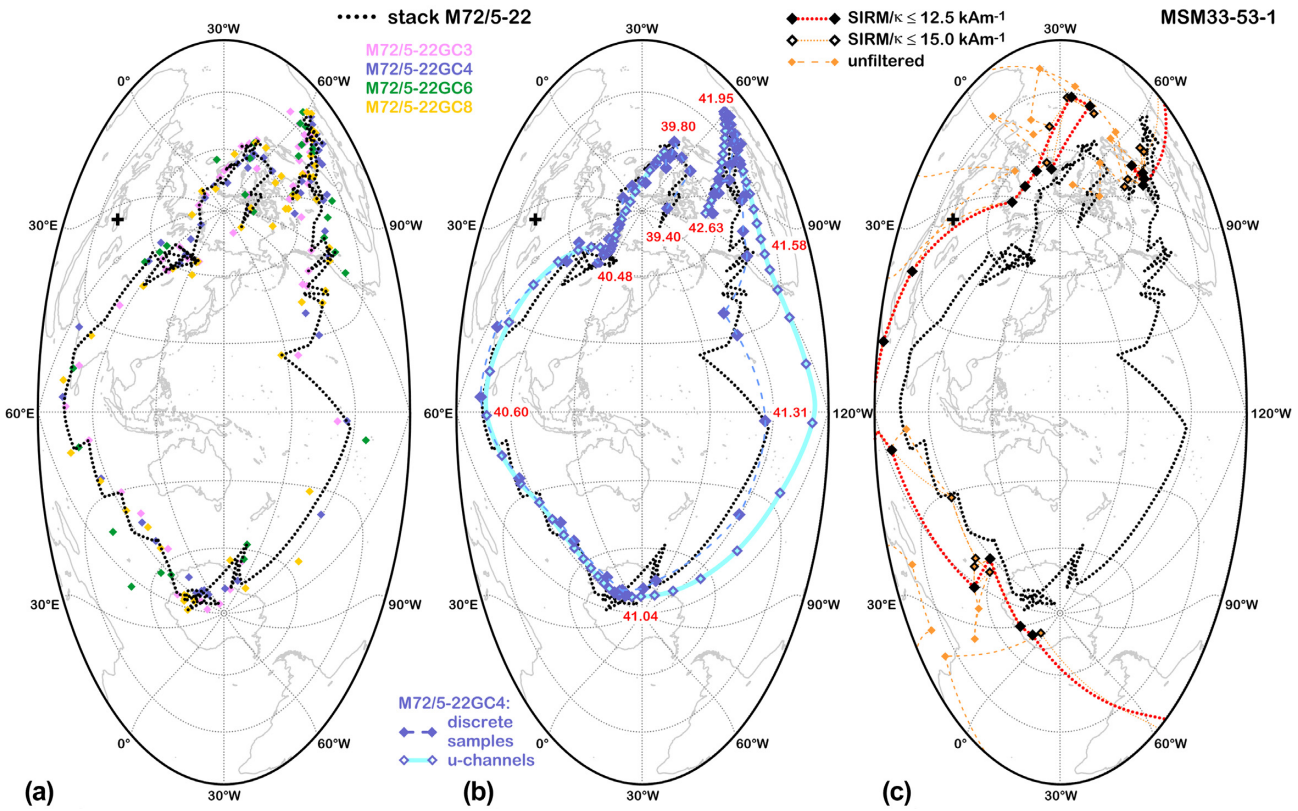

Figure 10. Movement of virtual geomagnetic poles (VGPs) from the study site in the SE Black Sea (black cross) during the Laschamps excursion from ~42.6 to 39.4 ka (Nowaczyk *et al*. 2012; polar Hammer-Aitoff projections). In all maps the VGP path of the stacked data from site M72/5–22 is plotted as black dotted lines. In (a) VGP positions obtained from the four individual M72/5–22 cores are marked by diamonds with their colours referring to the colour in the list of core numbers. In (b) the VGP path obtained from single core M72/5–22GC4 based on U-channels (open blue diamonds, light blue solid line) is compared to VGPs obtained from discrete samples (closed blue diamonds, blue dashed line) from this core. Red numbers in are ages of VGP positions given in ka. In (c) VGPs from new core MSM33–53-1 are shown from unfiltered data (small filled orange diamonds), from samples with SIRM/k_{LF} ≤ 15.0 kAm^{-1} (big black open diamonds), and from samples with SIRM/k_{LF} ≤ 12.5 kAm^{-1} (big black filled diamonds; see Section 3.2). VGPs are connected by lines on great circles.

excluding many samples whose palaeomagnetic information was biased by anomalous directions carried by greigite. In addition, declinations in core M72/5–25GC1, between 40 and 39 ka, are affected by some inexplicable distortions (question marks, Fig. 11b). At least, the reversed phase of the Laschamps excursion (red dotted horizontal lines) is documented by a few samples with declinations around 180° and shallow to steep negative inclinations in cores M72/5–25GC1 and MSM33–53-1. The clear field recovery during that phase to about 25 per cent of today's field intensity (see also Liu *et al.* 2020), documented at best in cores from site M72/5–22 (Fig. 11c), is only seen in core M72/5–25GC1. Here, core MSM33–53-1 is lacking too much data. The temporal field maximum of the fully reversed phase of the Laschamps excursion is also nicely documented in the U-channel record from core M72/5–22GC4, despite the fairly strong smoothing by the magnetometer's wide sensor characteristics. Due to technical reasons no ARM could be measured on the U-channels. Therefore, the NRM at 30 mT normalized by a low-pass filtered susceptibility record was used to estimate the palaeointensity, which fits very well to the slope NRM/ARM palaeointensity record derived from discrete samples. Two gaps are visible in the U-channel record from core M72/5–22GC4, one at around 43.0 ka and one at around 39.5 ka. Both are due to anomalous data from greigite bearing intervals (see Fig. 9). In addition, at the N-R transition, the declination record from U-channels contains values which are not present in the high-resolution discrete sample record. This is due to averaging across quickly changing directions, such as described also by Philippe *et al.* (2018), comparing artificial U-channel data with discrete sample data, or by Sagnotti *et al.* (2016), discussing fast directional changes related to the Matuyama-Brunhes reversal recorded in U-channels.

The Laschamps excursion as recorded in Black Sea sediments is not symmetrical. The field minimum before the final N-R transition is much deeper and broader than the minimum associated with R-N transition (Fig. 11c). Inclinations are also much shallower before the reversed phase of the Laschamps excursion than they are afterwards (Fig. 11a), while declinations in both cases reach almost 90°W. Actually this asymmetry is due to a pre-excursional feature, with VGPs migrating to the Caribbean first, with VGP latitudes as low as 15°N, before moving to the Antarctic area. This is more notably seen in the more common equatorial Hammer-Aitoff projection (Fig. 12) than in the unusual polar projection of the data (Fig. 10). Fig. 12 also shows VGP data from core CH89–9P (Lund *et al.* 2005) from the North Atlantic, directly sited on the VGP track of the Black Sea data. However, transitional VGP positions related to this site, shown as a blue line with short dashes, do not coincide with the Black Sea VGP track. The same can be stated for VGPs calculated from ODP Site 1233 in the SE Pacific (Lund *et al.* 2006), shown as red lines with long dashes in Fig. 12. As indicated by the arrows parallel to the VGP paths, the transitional VGPs from this southern hemisphere site are even moving in the opposite direction,

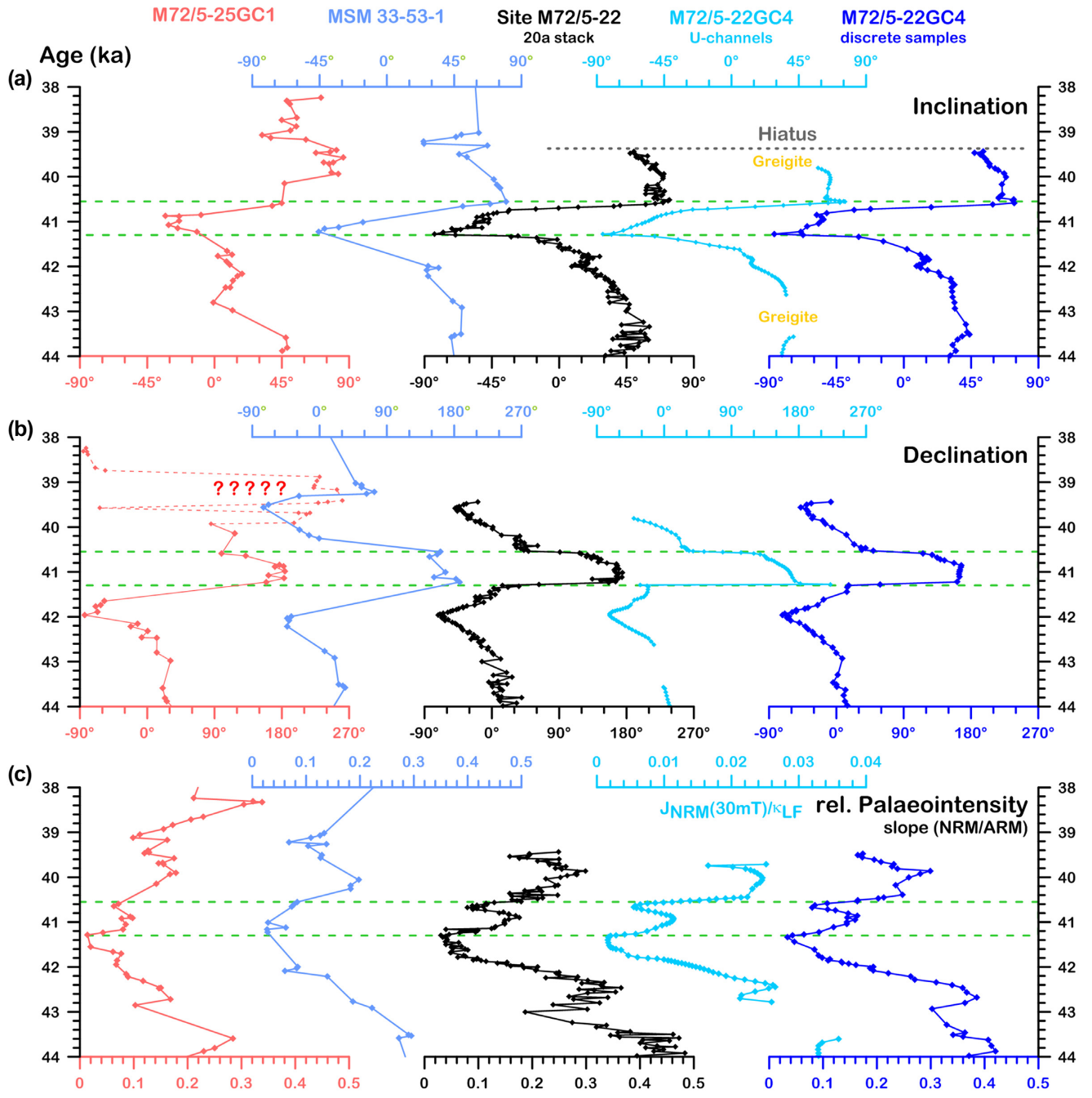

Figure 11. Compilation of time series of the Laschamps excursion for the time interval from 44 to 38 ka derived from SE Black Sea sediments. Inclination (a), declination (b), and relative palaeointensity (c) from individual cores M72/5–25GC1 and MSM33–53-1 (left-hand panel) and from core M72/5–22GC4, both from U-channels and discrete samples (right-hand panel), are shown together with the stacked data from site M72/5–22 (middle panel). Results from MSM33–53-1 are shown from samples with SIRM/$k_{LF} \leq 12.5$ kAm^{-1}. Question marks indicate doubtful declinations, though not affected by greigite, in core M72/5–25GC1, not seen in the (fragmentary) record from MSM33–53-1 from about the same site. As indicated in (a), gaps in the U-channel data from core M72/5–22GC4 are due to eliminated intervals with anomalous directions carried by greigite. The horizontal green dashed lines mark the totally reversed field during the Laschamps excursion in the Black sea area. Data from site M72/5–22 are cut off due to a hiatus starting at 39.4 ka, indicated by the horizontal black dotted line (only in a).

when compared to the tracks from the northern hemisphere sites. Also the VGP movement during the reversed phase (VGP latitudes higher than 45°S) appear to be much more dynamic, when compared to VGP positions calculated from the Black Sea record (Fig. 12). VGP calculation assumes a strictly dipolar magnetic field with its axis being tilted in various directions. Therefore, if the geomagnetic field would have been dominated by a tilted dipole, VGPs for the same time slice but from different sites have to cluster in the same area on the globe. Obviously, this is not the case for both polarity transitions of the Laschamps excursion. Therefore, this is a clear indication that the Earth magnetic field was dominated by multipolar features, instead of a tilting dipole, during the transitional phases of

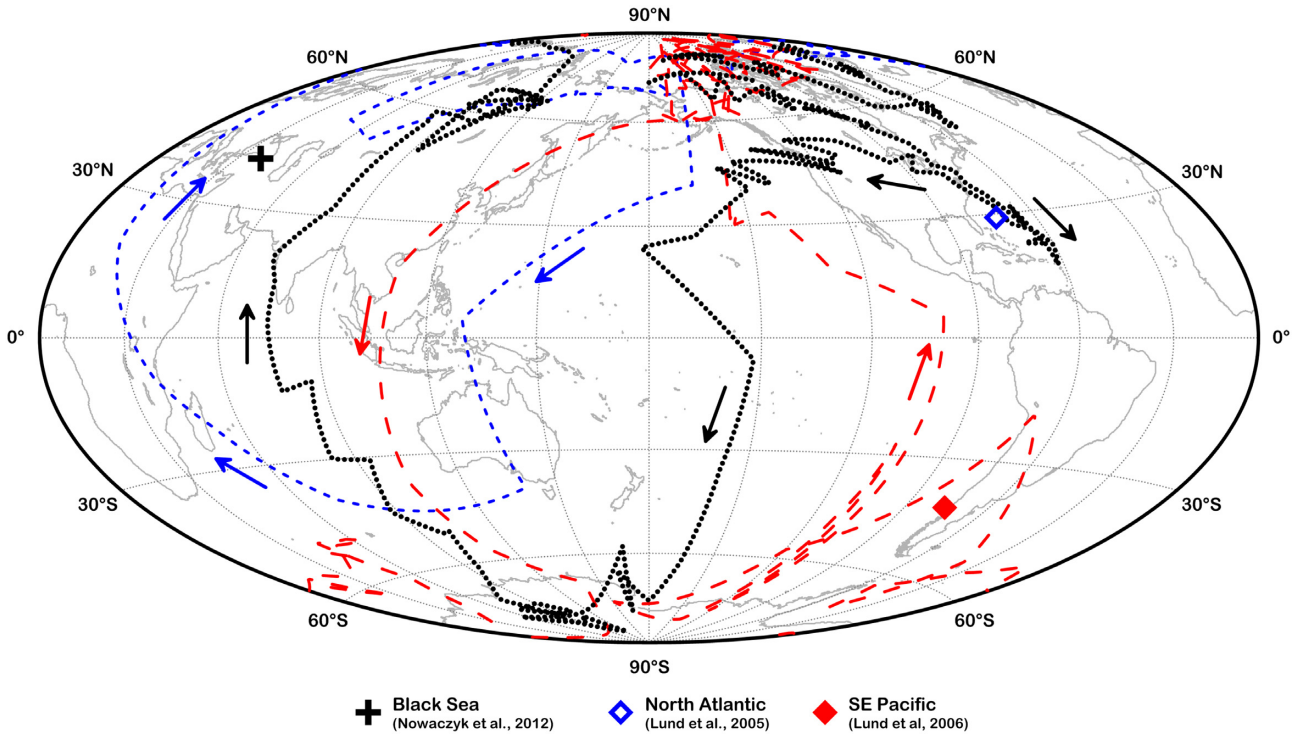

Figure 12. Comparison of VGP paths during the Laschamps excursion from three different sites in equatorial Hammer-Aitoff projection: black bold dotted line—Black Sea (Nowaczyk *et al.* 2012; this study); blue line with short dashes—North Atlantic, core CH89–9P (Lund *et al.* 2005); red line with long dashes—Southeast Pacific, ODP Site 1233 (Lund *et al.* 2006). Southward directed arrows mark the N-R transition at the onset of the excursion while northward directed arrows mark the terminating R-N transition. The partly opposing moving directions of the VGPs from the three different sites clearly indicate a multipolar field configuration at least during the transitional phases of the Laschamps excursion (see Panovska *et al.* 2019).

the Laschamps excursion. A new field model for this situation has been provided by Panovska *et al.* (2019), comprising, beside others, data shown in Fig. 12.

5 CONCLUSIONS

In summary, high-resolution discrete sample data from core MSM33–53-1 and U-channel data from core M727/5–22GC4 both are more or less affected by greigite. Although sediments from site M72/5–22 are much less contaminated, the smearing effect caused by the magnetometer's wide sensor characteristics required the elimination of data intervals of at least 15 cm length from the U-channel record (see Fig. 9), where greigite was suspected to spoil the palaeomagnetic data. A magnetometer with narrow pick-up coils still might require the elimination of 7–8 cm wide intervals, when the half-widths are half as wide (5 cm) compared to the one used for this study (9–10 cm). The U-channel directional data from core M72/5–22GC4 is also biased from averaging across fast changing field directions at the N-R transition of the Laschamps polarity excursion, resulting in an offset in the related VGP path of ∼30° in longitude, when compared to VGPs obtained from discrete samples from all four cores from site M72/5–22 (see Fig. 10). Thus, studying fast geomagnetic field variations, such as excursions and reversals, by U-channels appears to be problematic in some cases, as also postulated by Philippe *et al* (2018). In contrast, discrete samples taken at high-resolution obviously are the better choice, especially in the case of the studied Black Sea sediments. Non-stratiform occurring greigite could be specifically eliminated from the palaeomagnetic record, leaving only small gaps where greigite is only sporadically distributed in the sediments. In stratigraphic records massively impregnated by greigite, such as the ones from core MSM33–53-1 and M72/5–25GC1, elimination of greigite-bearing (discrete) samples left partly only a fragmentary record. But, at least, the major features in direction and relative palaeointensity even from geomagnetic excursions can be recognized still, providing important stratigraphic tie points.

ACKNOWLEDGEMENTS

We thank S. Plewe, M. Duwe, T. Moldenhawer and F. Brendel for their technical and logistical help during processing and subsampling of the cores. We also thank the captains and crews of *RV Meteor*, cruise M72/5 and *RV Maria S. Merian*, cruise MSM33, for their efforts in providing optimal scientific working conditions. We also appreciate the constructive comments and suggestions by two anonymous reviewers. This work was partly funded by the German Research Foundation (Deutsche Forschungsgemeinschaft, DFG SPP 1266 'INTERDYNAMIC' grants AR 367/9–1 and AR 367/9–2), the Gary Comer Science and Education Foundation, U.S.A. and the Chinese Scholarship Council (CSC grant No. 201506180060).

DATA AVAILABILITY STATEMENT

Palaeomagnetic data sets from cores MSM33–53-1, M72–5-22GC4, M72–5-25GC1 are available via GFZ Data Services, Nowaczyk *et al.* (2020), https://doi.org/10.5880/GFZ.4.3.2020.002.

REFERENCES

Bahr, A., Lamy, F., Arz, H., Kuhlmann, H. & Wefer, G., 2005. Late glacial to Holocene climate and sedimentation history in the NW Black Sea, *Mar. Geol.,* **214,** 309–322.

Bonhommet, N. & Babkine, J., 1967. Sur la présence d'aimantations inversèe dans la Chaîne des Puys, *C.R. Acad. Sci. Paris,* **264,** 92–94.

Brachfield, S.A., Kissel, C., Laj, C. & Mazaud, A., 2004. Behaviour of u-channels during acquisition and demagnetization of remanence: implications for paleomagnetic and rock magnetic measurements, *Phys. Earth Planet. Inter.,* **145,** 1–8.

Cassata, W.S., Singer, B.S., Liddicoat, J.C. & Coe, R.S., 2010. Reconciling discrepant chronologies for the geomagnetic excursion in the Mono Basin, California: Insights from new $^{40}Ar/^{39}Ar$ dating experiments and a revised relative paleointensity correlation, *Quat. Geochron.,* **5,** 533–543.

Channell, J.E.T., 2006. Late Brunhes polarity excursions (Mono Lake, Laschamp, Iceland Basin and Pringle Falls) recorded at ODP Site 919 (Irminger Basin), *Earth Planet. Sci. Lett.,* **244,** 378–393.

Channell, J.E.T., Singer, B.S. & Jicha, B.R., 2020. Timing of Quaternary geomagnetic reversals and excursions in volcanic and sedimentary archives, *Quat. Sci. Rev.,* **228,** 106114.

Croudace, I.W., Rindby, A. & Rothwell, R.G., 2006. ITRAX: description and evaluation of a new multi-function X-ray core scanner, *Geol. Soc. (Lond.) Spec. Publ.,* **267,** 51–63.

Cullen, V.L., Smith, V.C. & Arz, H.W., 2014. The detailed tephrostratigraphy of a core from the south-east Black Sea spanning the last ∼60 ka, *J. Quat. Sci.,* **29,** 675–690.

Dansgaard, W. *et al.*, 1993. Evidence for general instability of past climate from a 250-kyr ice-core record, *Nature,* **364,** 218–220.

Dekkers, M.J., Langereis, C.G., Vriend, S.P., van Santvoort, P.J.M. & de Lange, G.J., 1994. Fuzzy c-means cluster analysis of early diagenetic effects on natural remanent magnetisation acquisition in a 1.1 Myr piston core from the Central Mediterranean, *Phys. Earth Planet. Inter.,* **85,** 155–171.

Denham, C.R. & Cox, A., 1971. Evidence that the Laschamp event did not occur 13300–30400 years ago, *Earth Planet. Sci. Lett.,* **13,** 181–190.

De Vivo, B., Rolandi, G., Gans, P.B., Calvert, A., Bohrson, W.A., Spera, F.J. & Belkin, H.E., 2001. New constraints on the pyroclastic eruptive history of the Campanian volcanic Plain (Italy), *Mineral. Petrol.,* **73,** 47–65.

Fabbro, G.N., Druitt, T.H. & Scaillet, S. 2013. Evolution of the crustal magma plumbing system during the build-up to the 22-ka caldera-forming eruption of Santorini (Greece), *Bull Volc*., **75**(12), 767.

Fisher, R.A., 1953. Dispersion on a sphere, *Proc. R. Soc. Lond., A,* **217,** 295–305.

Giaccio, B., Hajdas, I., Isaia, R., Deino, A. & Nomade, S. 2017. High-precision 14C and 40Ar/39Ar dating of the Campanian Ignimbrite (Y-5) reconciles the time-scales of climatic-cultural processes at 40 ka, *Sci. Rep.,* **7,** doi:10.1038/srep45940.

Gillot, P.Y., Labeyrie, J., Laj, C., Valladas, G., Guerin, G., Poupeau, G. & Delibrias, G., 1979. Age of the Laschamp paleomagnetic excursion revisited, *Earth Planet. Sci. Lett.,* **42,** 444–450.

Guillou, H., Singer, B.S., Laj, C., Kissel, C., Scaillet, S. & Jicha, B.R., 2004. On the age of the Laschamp excursion, *Earth Planet. Sci. Lett.,* **227,** 331–343.

Guyodo, Y., Channell, J.E.T. & Thomas, R.G., 2002. Deconvolution of u-channel paleomagnetic data near geomagnetic reversals and short events, *Geophys. Res. Lett.,* **29**(17), 1845.

Höflmayer, F., 2012. The date of the Minoan Santorini eruption: quantifying the "offset", *Radiocarbon,* **54,** 435–448.

Jackson, M., Bowles, J.A., Lasc, I. & Solheid, P., 2010. Deconvolution of u channel magnetometer data: experimental study of accuracy, resolution, and stability of different inversion methods, *Geochem. Geophys. Geosyst.,* **11**(7), doi:10.1029/2009GC002991.

Kirschvink, J.L., 1980. The least-squares line and plane and the analysis of palaeomagnetic data, *Geophys. J. R. astr. Soc.,* **62,** 699–718.

Kissel, C., Guillou, H., Laj, C., Carracedo, J.C., Nomade, S., Perez-Torrado, F. & Wandres, C., 2011. The Mono Lake excursion recorded in phonolitic lavas from Tenerife (Canary Islands): Paleomagnetic analyses and coupled K/Ar and Ar/Ar dating, *Phys. Earth Planet. Inter.,* **187,** 232–244.

Kornprobst, J. & Lénat, J.-F., 2019. Changing name for Earth's changing poles, *Eos,* 100, https://doi.org/10.1029/2019EO117913.

Kwiecien, O., Arz, H.W., Lamy, F., Wulf, S., Bahr, A., Röhl, U. & Haug, G.H.,2008. Estimated reservoir ages of the Black Sea since the last glacial, *Radiocarbon,* **50,** 1–20.

Laj, C., Guillou, H. & Kissel, C., 2014. Dynamics of the earth magnetic field in the 10–75 kyr period comprising the Laschamp and Mono Lake excursions : new results from the French Chaîne des Puys in a global perspective, *Earth Planet. Sci. Lett.,* **387,** 184–197.

Lamy, F., Arz, H.W., Bond, G.C., Bahr, A. & Petzold, J., 2006. Multicentennial-scale hydrological changes in the Black Sea and northern Red Sea during the Holocene and the Arctic/North Atlantic Oscillation, *Paleoceanography,* **21,** PA1008, doi:10.1029/2005PA001184.

Liddicoat, J.C. & Coe, R.S., 1979. Mono Lake geomagnetic excursion, *J. geophys. Res.,* **84,** 261–271.

Liu, J., Nowaczyk, N.R., Frank, U. & Arz, H.W., 2018. A 20–15 ka high-resolution paleomagnetic secular variation record from Black Sea sediments – no evidence for the 'Hilina Pali excursion'? *Earth Planet. Sci. Lett.,* **492,** 174–185.

Liu, J., Nowaczyk, N.R., Frank, U. & Arz, H.W., 2019. Geomagnetic paleosecular variation record spanning from 40 to 20 ka - implications for the Mono Lake excursion from Black Sea sediments, *Earth Planet. Sci. Lett.,* **509,** 114–124.

Liu, J., Nowaczyk, N.R., Panovska, S., Korte, M. & Arz, H., 2020. The Norwegian-Greeland Sea, the Laschamps and the Mono Lake excursions recorded in a Black Sea sedimentary sequence spanning from 68.9 to 14.5 ka, *J. Geophys. Res.,* **125,** e2019JB019225, doi:10.1029/2019JB019225.

Lund, S.P., Liddicoat, J.C., Lajoie, K.R., Henyey, T.L. & Robinson, S.W., 1988. Paleomagnetic evidence for long-term (104 year) memory and periodic behavior in the earth's core dynamo process, *Geophys. Res. Lett.,* **15,** 1101–1105.

Lund, S.P., Schwartz, M., Keigwin, L. & Johnson, T., 2005. Deep-sea sediment records of the Laschamp geomagnetic field excursion (∼41,000 calendar years before present), *J. Geophys. Res.,* **110,** B04101, doi:10.1029/2003JB002943.

Lund, S.P., Stoner, J.S., Channell, J.E.Z. & Acton, G., 2006. A summary of Brunhes paleomagnetic field variability recorded in Ocean Drilling Program cores, *Phys. Earth Planet. Inter.,* **156,** 194–204.

Major, C.O., Goldstein, S.L., Ryan, W.B.F., Lericolais, G., Piotrowski, A.M. & Hajdas, I., 2006. The co-evolution of Black Sea level and composition through the last deglaciation and its paleoclimatic significance, *Quat. Sci. Rev.,* **25,** 2031–2047.

Merrill, R. T. & McFadden, P. L.(1999). Geomagnetic polarity transitions, *Rev. Geophys.,* **37**(2), 201–226.

Nagy, E.A. & Valet, J.-P., 1993. New advances for paleomagnetic studies of sediment cores using U-channels, *Geophys. Res. Lett.,* **20**(8), 671–674.

Nowaczyk, N.R., 2011. Dissolution of titanomagnetite and sulphidization in sediments from Lake Kinneret, Israel, *Geophys. J. Int.,* **187,** 34–44.

Nowaczyk, N.R., Antonow, M., Knies, J. & Spielhagen, R.F., 2003. Further rock magnetic and chronostratigraphic results on reversal excursions during the last 50 ka as derived from northern high latitudes and discrepancies in precise AMS 14 C dating, *Geophys. J. Int.,* **155,** 1065–1080.

Nowaczyk, N.R., Arz, H.W., Frank, U., Kind, J. & Plessen, B., 2012. Dynamics of the Laschamp geomagnetic excursion from Black Sea sediments, *Earth Planet. Sci. Lett.,* **351–352,** 54–69.

Nowaczyk, N.R., Frank, U., Kind, J. & Arz, H.W., 2013a. A high-resolution paleointensity stack of the past 14 to 68 ka from black sea sediments, *Earth Planet. Sci. Lett.,* **384,** 1–16.

Nowaczyk, N.R. *et al.*, 2013b. Chronology of Lake El'gygytgyn sediments – a combined magnetostratographic, palaeoclimatic and orbital tuning study based on multi-parameter analysis, *Clim. Past,* **9,** 2413–2432.

Nowaczyk, N.R., Liu, J., Frank, U. & Arz, H.W., 2018. A high-resolution paleosecular variation record from Black Sea sediments indicating fast directional changes associated with low field intensities during marine isotope stage (MIS) 4, *Earth Planet. Sci. Lett.,* **484,** 15–29.

Nowaczyk, N.R., Liu, J. & Arz, H.W. 2020, Paleo- and rock magnetic data from cores MSM33-53-1, M72-5-22GC4, M72-5-25GC1, Black Sea, GFZ Data Services, https://doi.org/10.5880/GFZ.4.3.2020.002.

Oda, H. & Shibuya, H., 1996. Deconvolution of long-core paleomagnetic data of Ocean Drilling Program by Akaike's Bayesian Information Criterion minimization, *J. geophys. Res.,* **101**(B2), 2815–2834.

Oda, H. & Xuan, C., 2014. Deconvolution of continuous paleomagnetic data from pass-through magnetometer: a new algorithm to restore geomagnetic and environmental information based on realistic optimization, *Geochem. Geophys. Geosyst.,* **15,** 3907–3924.

Panovska, S., Korte, M. & Constable, C.G., 2019. One hundred thousand years of geomagnetic field evolution, *Rev. Geophys.,* **57,** 1289–1337.

Philippe, É.G.H., Valet, J.-P., St-Onge, G. & Thevarasan, A., 2018. Are paleomagnetic records from U-channels appropriate for studies of reversals and excursions? *Geochem. Geophys. Geosyst.,* **19,** 4130–4142.

Plenier, G., Valet, J.-P., Guérin, G., Lefèvre, J.-C., LeGoff, M. & Carter-Stiglitz, B., 2007. Origin and age of the directions recorded during the Laschamp event in the Chaîne des Puys, *Earth Planet. Sci. Lett.,* **259,** 414–431.

Pyle, D.M., Ricketts, G.D., Margari, V., van Andel, T., Sinitsyn, A.A., Praslov, N.D. & Lisitsyn, S., 2006. Wide dispersal and deposition of distal tephra during the Pleistocene 'Campanian Ignimbrite/Y5' eruption, Italy, *Quat. Sci. Rev.,* **25,** 2713–2728.

Roberts, A.P., 2006. High-resolution magnetic analysis of sediment cores: Strengths, limitations and strategies for maximizing the values of long-core magnetic data, *Phys. Earth. Planet. Inter.,* **156,** 162–178.

Roberts, A.P., 2008. Geomagnetic excursions: knowns and unknowns, *Geophys. Res. Lett.,* **35,** 1–7.

Roberts, A.P., Chang, L., Rowan, C.J., Horng, C.-S. & Florindo, F., 2011. Magnetic properties of sedimentary greigite (Fe_3S_4): an update, *Rev. Geophys.,* **49,** RG1002, doi:10.1029/2010RG000336.

Ron, H., Nowaczyk, N.R., Frank, U., Schwab, M.J., Naumann, R., Striewski, B. & Agnon, A., 2007. Greigite detected as dominating remanence carrier in Late Pleistocene sediments, Lisan formation, from Lake Kinneret (Sea of Galilee), Israel, *Geophys. J. Int.,* **170,** 117–131.

Sagnotti, L., Giaccio, B., Liddicoat, J.C., Nomade, S., Renne, P.R., Scardia, G. & Sprain, C.J., 2016. How fast was the Matuyama-Brunhes geomagnetic reversal? A new subcentennial record from the Sulmona Basin, central. Italy, *Geophys. J. Int.,* **204,** 798–812.

Shumilovskikh, L.S. *et al.*, 2012. Vegetation and environmental dynamics in the southern Black Sea region since 18kyr BP derived from the marine core 22-GC3, *Palaeogeogr. Palaeoclimatol. Palaeoecol.,* **337–338,** 177–193.

Shumilovskikh, L.S., Marret, F., Fleitmann, D., Arz, H.W., Nowaczyk, N. & Behling, H., 2013. Eemian and Holocene sea-surface conditions in the southern Black Sea: organic-walled dinoflagellate cyst record from core 22-GC3, *Mar. Micropaleontol.,* **101,** 146–160.

Snowball, I.F., 1997. Gyroremanent magnetization and the magnetic properties of greigite-bearing clays in southern Sweden, *Geophys. J. Int.,* **129,** 624–636.

Snowball, I. & Thompson, R., 1988. The occurrence of greigite in sediments from Loch Lomond, *J. Quat. Sci.,* **3**(2), 121–125.

Soulet, G., Menot, G., Bayon, G., Rostek, F., Ponzevera, E., Toucanne, S., Lericolais, G. & Bard, E., 2013. Abrupt drainage cycles of the Fennoscandian Ice Sheet, *Proc. Natl. Acad. Sci.,* **110,** 6682–6687.

Svensson, A. *et al.*, 2008. A 60 000 year Greenland stratigraphic ice core chronology, *Clim. Past, Eur. Geosci. Un.,* **4,** 47–57.

Weeks, R., Laj, C., Endignoux, L., Fuller, M., Roberts, A., Manganne, R., Blanchard, E. & Goree, W., 1993. Improvements in long-core measurement techniques: applications in palaeomagnetism and palaeoceanography, *Geophys. J. Int.,* **114,** 561–662.

Wegwerth, A. *et al.*, 2014. Meltwater events and the Mediterranean reconnection at the Saalian-Eemian transition in the Black Sea, *Earth Planet. Sci. Lett.,* **404,** 124–135.

Wegwerth, A., Ganopolski, A., Ménot, G., Kaiser, J., Dellwig, O., Bard, E., Lamy, F. & Arz, H.W., 2015. Black Sea temperature response to glacial millennial-scale climate variability, *Geophys. Res. Lett.,* **42,** 8147–8154.

Wegwerth, A., Kaiser, J., Dellwig, O., Shumilovskikh, L.S., Nowaczyk, N.R. & Arz, H.W., 2016. Northern hemisphere climate control on the environmental dynamics in the glacial Black Sea "Lake", *Quat. Sci. Rev.,* **135,** 41–53.

Xuan, C. & Oda, H., 2015. UDECON: deconvolution optimization software for restoring high-resolution records from pass-through paleomagntic measurements, *Earth Planets Space,* **67,** 183.

Xuan, C. & Oda, H., 2019. Sensor response estimate and cross calibration of paleomagnetic measurements on pass-through superconducting rock magnetometers, *Geochem. Geophys. Geosyst.,* **20,** 4676–4692.